

A point to point response to the reviewers' comments

Thank you for the reviewers' comments on our manuscript entitled "Ozone affected by a succession of four landfall typhoons in the Yangtze River Delta, China: major processes and health impacts" (acp-2020-554). Those constructive comments are all valuable for revising and improving our manuscript, as well as the important guiding significance to our researches. We have studied those comments carefully and have made correction which we hope to meet with approval. Here are point to point responses (in blue colored). Accordingly, we also revised manuscript (in red colored).

Anonymous Referee #1:

General comments

This research is talking about an interesting topic. Ozone pollution episodes caused by the landfall typhoon were analyzed based on typical cases in the Yangtze River delta in China. This study provided an insight into the characteristics of the occurrence of ozone pollution and the changes in O₃ concentrations during the special synoptic system. I think this paper is well-organized and presenting an important schematic diagram.

Response: we would like to express our great appreciation to you for your encouragement.

Specific comments

Here are some questions listed in the below, which need further addressing in the modified version:

Response: we thank the reviewer for the careful reading and the constructive comments, which are really important to improving our manuscript. We have carefully revised our manuscript based on the reviewer's comments.

1. Section 3.1, Figure2, since the influences of the typhoon cases are special in 2018, could the authors add summertime ozone concentrations in 2017 and 2019 (if the measurement data could be available) to compare with that in 2018 to show the roles clearer?

Response: Thanks for the constructive comment. We have accepted your suggestion, and carefully sorted out the O₃ concentrations as well as the typhoon information in summer from 2015 to 2019. We have included this information Supplement in this revised version. Also, we have revised our manuscript simultaneously. Please see lines 242-244 (Sect. 3.1) in the revised manuscript.

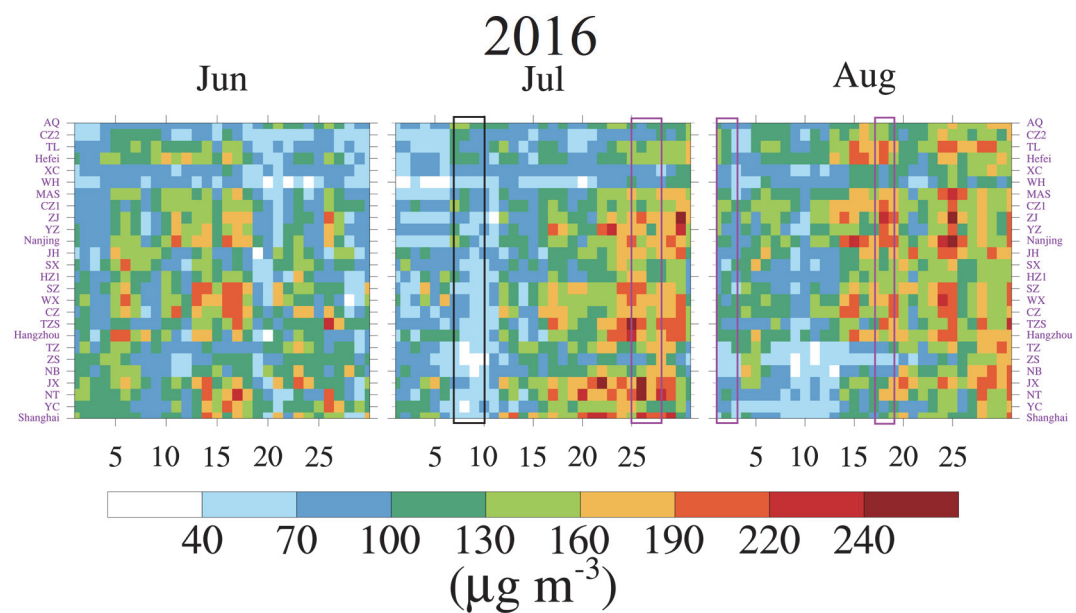
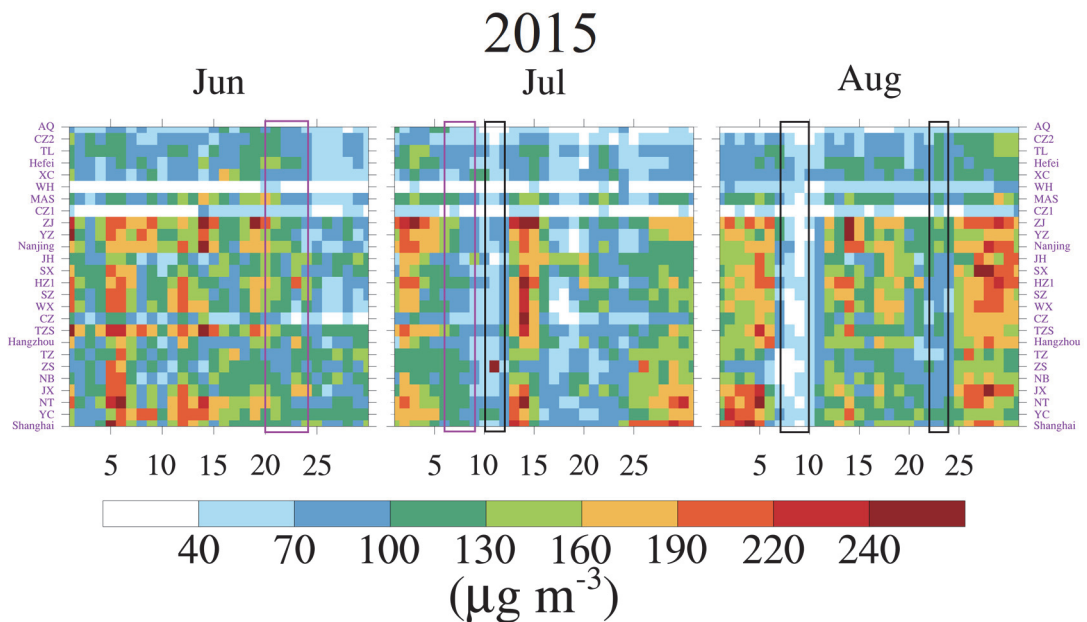
According to the conclusion of our paper, the moment that typhoon reaches the 24-h warning line is crucial. Thus, we list all the typhoons that can reach this warning line (Table R1), and mark the corresponding moment on the O₃ concentration map (Figure R1). Actually, similar phenomena can also occur in other years, not just in 2018. That is, O₃ pollution episodes tend to occur during the period from the end of a typhoon and the arrival of the next typhoon, and O₃ pollution occurs earlier in cities near the coastline (Figure R1: July in 2015, July in 2016, July in 2017, July and August in 2018, and August in 2019). O₃ concentrations are more sensitive to typhoons landed in Fujian (Zhejiang) compared to those landed in Guangdong (Hainan). We choose 2018 because there are lots of landfall typhoons, and the landfall positions is further north in this year. Four consecutive landfall typhoons and four respective cities with different longitudes can provide a wealth of information about the mechanism of landfall typhoon affecting O₃ in the YRD. The major processes (the schematic diagram) in our paper may be universal as the similar phenomena can also occur in other years.

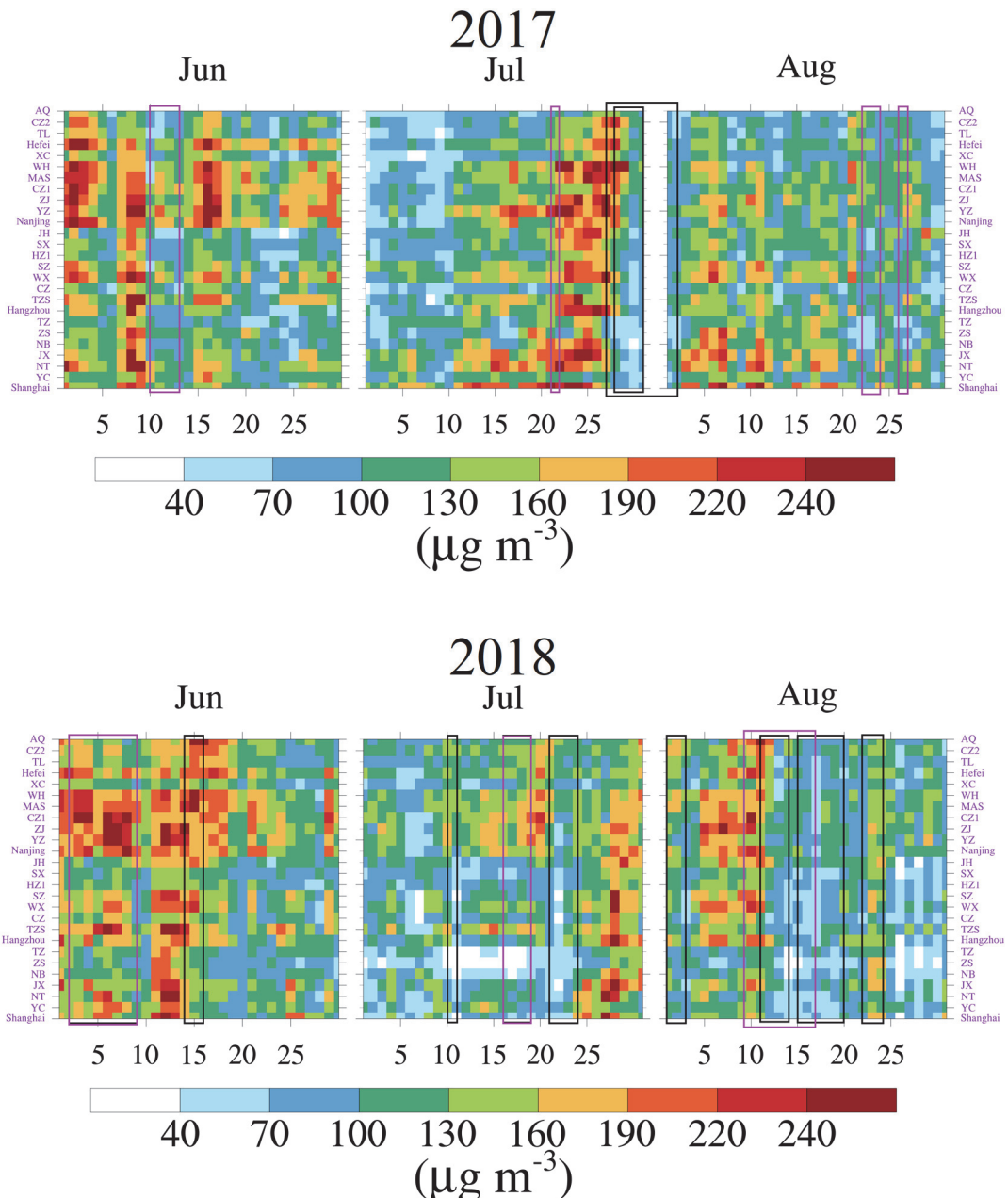
Table R1: Information on typhoons that can approach the 24-h warning line in the summer from 2015 to 2019.

Note. The start date is defined as the date of typhoon reaching the 24-h warning line, while the end

Year	Serial number	Name	Start date	End date	Whether typhoon landed?	Landfall position
2015	1508	Kujira	20 June	24 June	Yes	Hainan
	1509	Chan-hom	10 July	12 July	No	
	1510	Linfa	6 July	9 July	Yes	Guangdong
	1513	Soudelor	7 August	10 August	Yes	Fujian
	1515	Goni	22 August	24 August	No	
2016	1601	Nepartak	7 July	10 July	Yes	Fujian
	1603	Mirinae	25 July	28 July	Yes	Hainan
	1604	Nida	1 August	3 August	Yes	Guangdong
	1608	Dianmu	17 August	19 August	Yes	Guangdong
2017	1702	Merbok	10 June	13 June	Yes	Hong Kong
	1707	Roke	22 July	23 July	Yes	Hong Kong
	1709	Nesat	28 July	31 July	Yes	Fujian
	1710	Haitang	27 July	2 August	Yes	Fujian
	1713	Hato	22 August	24 August	Yes	Guangdong
	1714	Pakhar	26 August	27 August	Yes	Guangdong
2018	1804	Ewiniar	2 June	9 June	Yes	Guangdong
	1806	Gaemi	14 June	16 June	No	
	1808	Maria	10 July	11 July	Yes	Fujian
	1809	Son-tinh	16 July	19 July	Yes	Hainan
	1810	Ampil	21 July	24 July	Yes	Shanghai
	1812	Jongdari	1 August	3 August	Yes	Shanghai
	1814	Yagi	11 August	14 August	Yes	Zhejiang
	1816	Bebinca	9 August	17 August	Yes	Hainan
	1818	Rumbia	15 August	20 August	Yes	Shanghai
	1819	Soulik	22 August	24 August	No	
2019	1904	Mun	1 July	4 July	Yes	Hainan
	1905	Danas	17 July	20 July	No	
	1907	Wipha	30 July	3 August	Yes	Hainan
	1909	Lekima	7 August	13 August	Yes	Zhejiang
	1911	Bailu	23 August	25 August	Yes	Fujian

date is the date of typhoon leaving the 24-h warning line. Dates of typhoon reaching/leaving 24-h warning line also represent the generation/death dates of typhoon as long as the typhoon is active within the 24-h warning line.





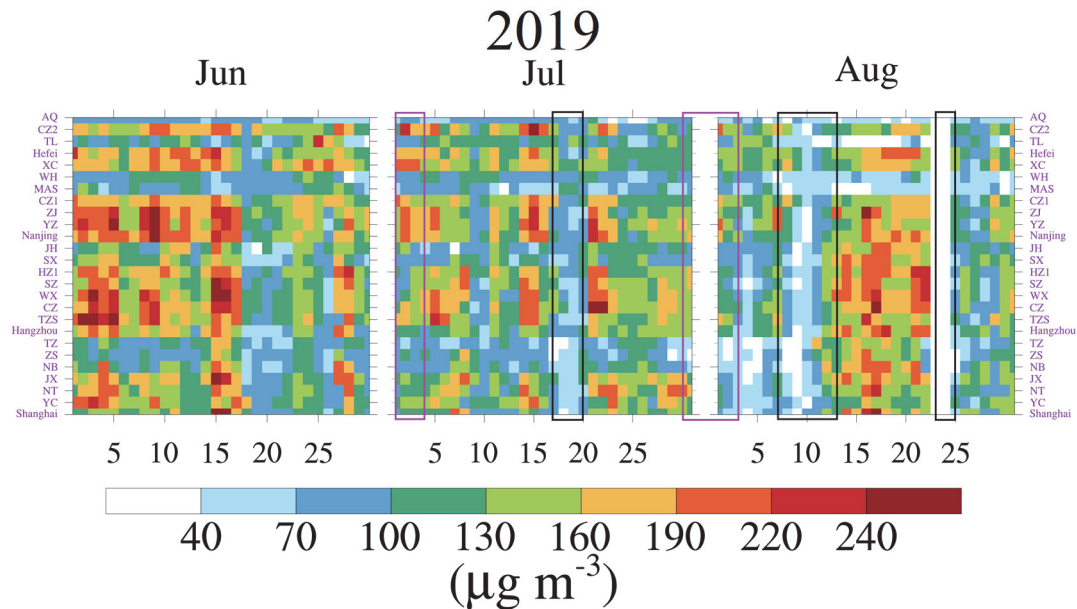


Figure R1. The MDA8 O₃ in 26 cities of the YRD in summer from 2015 to 2019. The open purple and blue boxes indicate that the affected region are mainly the Pearl River Delta and the Yangtze River Delta, respectively. The national ambient air quality standard for MDA8 O₃ is 160 $\mu\text{g m}^{-3}$ in China. These cities are sorted by longitude.

2. Section 3.2, Line 309, Here the authors mentioned the “coastal” region and “inland” region, what is the distance definition for them? Could you describe them here?

Response: Thanks for the constructive comment. We are sorry that we did not give specific definitions of “coastal” and “inland” region in the last version. By consulting relevant information, we find that “inland” region usually refer to the area more than 500 km from the coastline in geography. Thus, the words “coastal” and “inland” are indeed inappropriate here. We have changed the “coastal region” to “cities along the coastline”, and deleted the “inland regions” in our revised manuscript. Please see lines 327-328 (Sect. 3.2), 541 (Sect. 3.3.6) and 617-618 (Sect. 4) in the revised manuscript.

3. Section 3.3, Line 324, the representatives of the chosen cities should be addressed here, is it according to the distance off coastal lines?

Response: Thanks for the constructive comment. We are sorry that we did not explain why to select these cities, and we did not provide geographical information of these cities in our original

manuscript. This important information is given in our new manuscript, please see lines 341-344 (Sect. 3.3) in the revised manuscript.

We selected Shanghai (121.77°E, 31.12°N), Hangzhou (120.17°E, 30.23°N), Nanjing (118.80°E, 32.00°N) and Hefei (117.23°E, 31.87°N) for the following reasons:

- a. Shanghai is a megacity directly under the administration of China. Hangzhou, Nanjing and Hefei are the capital city of Zhejiang, Jiangsu and Anhui province, respectively. Pollution episodes in these cities can impact a large population.
- b. These cities are distributed at different longitudes in various distances to the east coast. Therefore, O₃ variations in these geographic locations during a typhoon landing can reflect the impact of typhoons on O₃ as typhoons continue to approach the mainland.
- c. During the typhoon, many observations were missing. We finally chose the data collected by the University of Wyoming (<http://weather.uwyo.edu/surface/>) due to its completeness and number of uses. However, the data only are available in these four cities in the Yangtze River Delta.

4. Section 3.3 Table 3, what is the situation for simulated precipitation compare with the observed one?

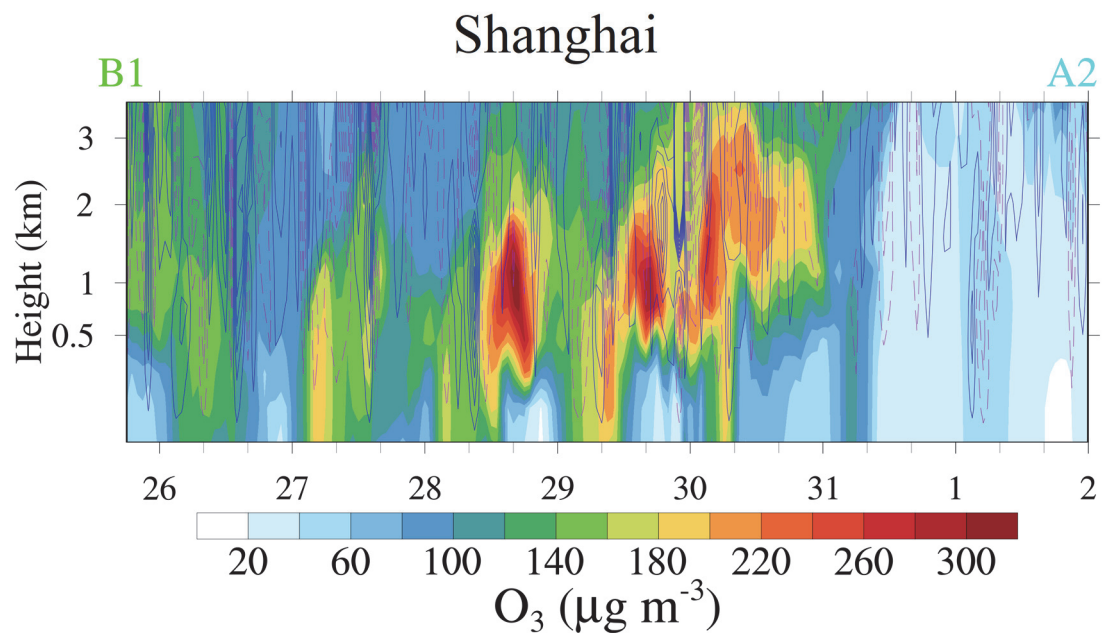
Response: Thanks for the constructive comment. We strongly agree that precipitation is important. However, precipitation data are not available in the data sets provided by the University of Wyoming. Their data only contain the variables of pressure, temperature, dew point, relative humidity, wind direction, wind speed and visibility. Therefore, we cannot make a comparison between the simulated and observed precipitation. We have discussed this limitation in line 143 in the revised manuscript. Future work can be done in comparing the simulated and observed precipitation.

5. Also, Line 386-388, the authors mentioned the high value center of O₃ appeared near altitude of 1km instead of near surface caused by the high photochemical production efficiency of ozone. What is the physical transport role in the high O₃ here?

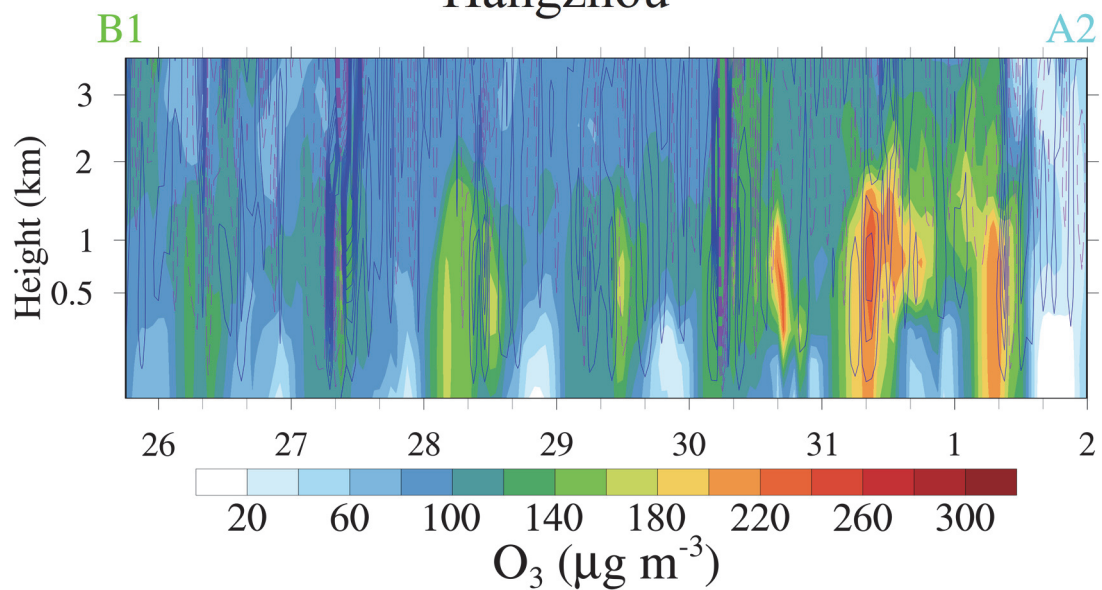
Response: Thanks for the constructive comment. According to your suggestion, we have added the physical role that causes high surface O₃, and largely reorganized the content in the revised manuscript. Please see lines 30-38 (Abstract), 410-422 (Sect. 3.3.2), 545-552 (Sect. 3.3.6) and 634-

641 (Sect. 4).

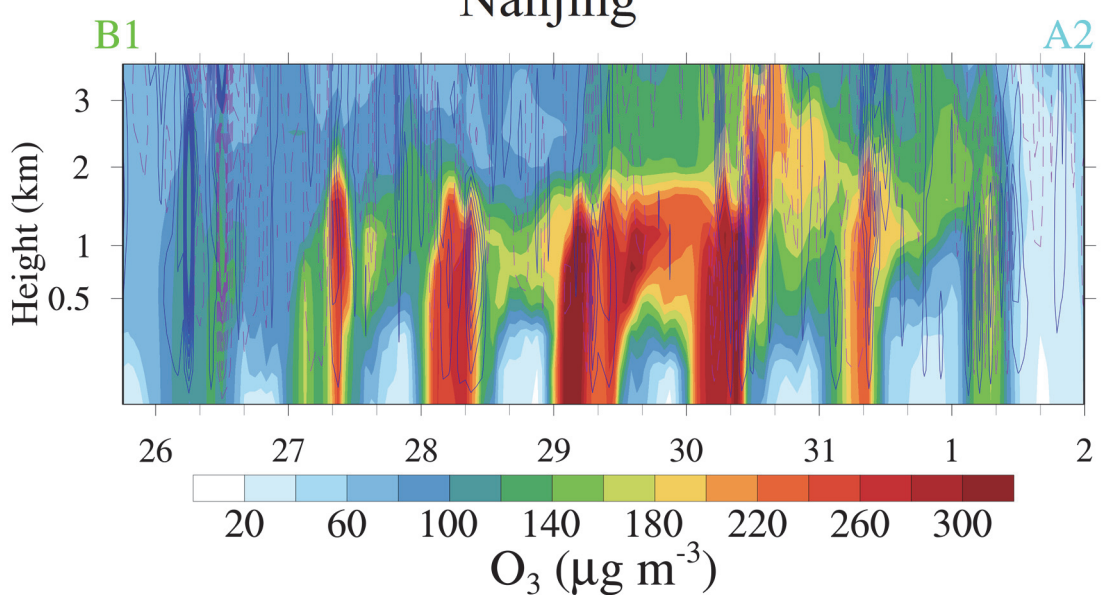
Figure R2 presents a fine map of temporal-vertical distribution of O₃ with vertical wind velocity over Shanghai, Hangzhou, Nanjing and Hefei during high O₃ pollution episodes, which may be helpful to study how high-level O₃ is transported to the surface. After typhoon, the downdraft airflows gradually became dominant, the atmosphere was stagnant, and the temperature rose. During the day, O₃ was produced by photochemical reactions, and high O₃ flooded the entire boundary layer due to a well-mixed boundary layer. Most of the O₃ remained in the residual layer (Surface O₃ was much lower due to NO_x titration) at night. By the second day, high O₃ in the residual layer can be transported to the surface by the downward airflows as the boundary layer gradually mixed. Combined with the newly generated O₃, high O₃ would be easy to appear on the surface.



Hangzhou



Nanjing



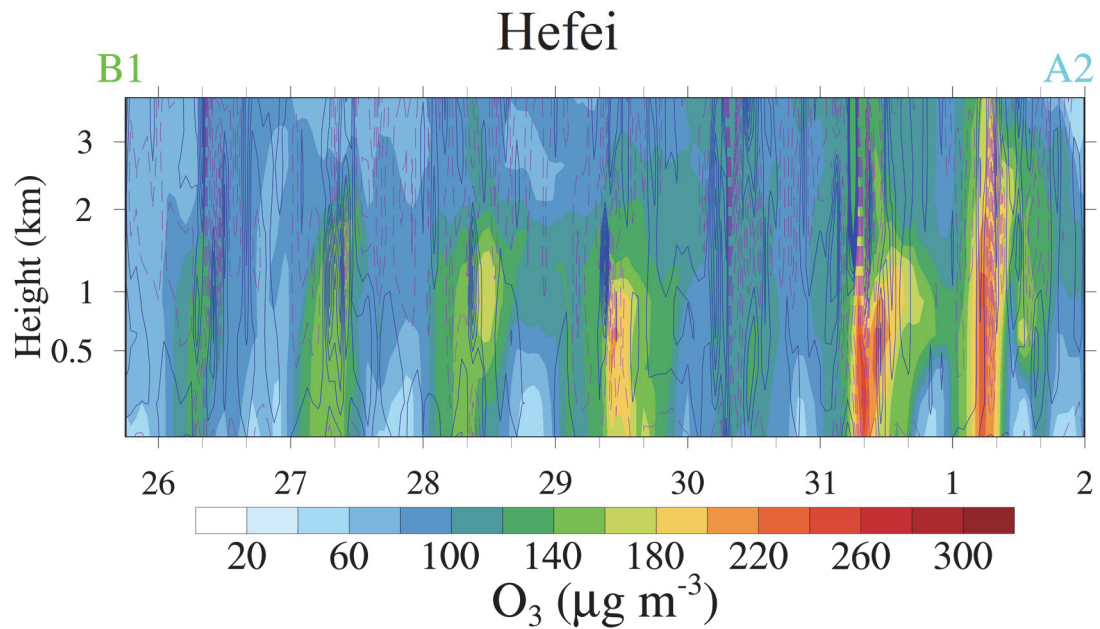


Figure R2: Temporal-vertical distribution of O_3 with vertical wind velocity over Shanghai, Hangzhou, Nanjing and Hefei. The dashed purple line and solid blue line indicate the downward airflows and upward airflows, respectively. The time refers to UTC.

6. Section 3.7, the evaluation on the premature mortalities induced by O_3 exposure are important, but here the authors did not give detailed methodologies or any reference about the estimation of premature mortalities. More details should be added here.

Response: We appreciate this constructive comment. In our revised manuscript, we have added a brief description of the methodology for the estimation of premature mortalities (The detailed calculation method can be found in Section 2.7 Estimate of health impacts), which makes the structure of the article more coherent. Please see lines 590-593 (Sect. 3.3) in the revised manuscript.

Technical corrections

1. Table 3: the authors need indicating o and s with “observation” and “simulation” as a note.

Response: Thanks for the constructive comment. We have added the note that \bar{O} and \bar{S} are the average value of observations and simulations in Table 3. Please see lines 370-371 (Table 3) in the revised manuscript.

1 **Ozone affected by a succession of four landfall typhoons in**
2 **the Yangtze River Delta, China: major processes and health**
3 **impacts**

4 Chenchao Zhan^{a,1}, Min Xie^{a,*}, Chongwu Huang^{a,1}, Jane Liu^{b,c}, Tijian Wang^a, Jane Liu^{b,e}, Meng
5 Xu^d, Chaoqun Ma^a, Jianwei Yu^e, Yumeng Jiao^f, Mengmeng Li^a, Shu Li^a, Bingliang Zhuang^a,
6 Ming Zhao^a, Dongyang Nie^a

7 ^a School of Atmospheric Sciences, Joint Center for Atmospheric Radar Research of CMA/NJU,
8 CMA-NJU Joint Laboratory for Climate Prediction Studies, Jiangsu Collaborative Innovation
9 Center for Climate Change, Nanjing University, Nanjing 210023, China

10 ^b College of Geographic Sciences, Fujian Normal University, 350007, Fuzhou, China

11 ^c Department of Geography and Planning, University of Toronto, Toronto, Ontario, Canada

12 ^d Jiangsu Provincial Climate Center, Nanjing 210009, China

13 ^e Jiangsu Provincial Meteorological Observatory, Nanjing 210008, China

14 ^f Department of Microbiology and Parasitology, Bengbu Medical College, Bengbu 233030, China

16 * Corresponding author. minxie@nju.edu.cn (M. Xie)

17 ¹ The third author can be considered as the co-first author

19 **Abstract:** Landfall typhoon can significantly affect O₃ in the Yangtze River Delta (YRD) region. In
20 this study, we investigate a unique case characterized by two multiday regional O₃ pollution
21 episodes related to four successive landfall typhoons in the summer of 2018 in the YRD. The results
22 show that O₃ pollution episodes mainly occurred during the period from the end of a typhoon to and
23 the arrival of the next typhoon. The time when a moment that typhoon reached the 24-h warning line
24 and the time when the last moment of typhoon dies away activity in the mainland China can be
25 roughly regarded as time nodes. Meanwhile, the variations of O₃ was related to the track, duration
26 and landing intensity of the typhoons. The impact of typhoons s on O₃ was like a wave superimposed
27 on the background of high O₃ concentration in the YRD in summer. When a typhoon was near the
28 24-h warning line before it landed the coast line of the YRD, the prevailing wind originally from
29 the ocean changed to from the inland, and transported lots of precursors from the polluted areas to
30 the YRD. Under influences of theWith typhoon, the low temperature, strong upward airflows, more

31 precipitation and wild wind ~~hindered occurrences of prevented~~ high O₃ episodes. After ~~the passing~~
32 ~~of the~~ typhoon, the air below the 700 hPa atmospheric layer was warm and dry, ~~and the downward~~
33 ~~airflows resumed. The low troposphere was filed with high concentration of O₃ due to O₃-rich air~~
34 ~~transported from the low stratosphere and strong photochemical reactions, which was conductive to~~
35 ~~the formation of O₃ from the abundance of precursors.~~ It is note-worthly that O₃ ~~was~~ mainly
36 generated in the middle of boundary layer (~ 1000 m) ~~instead of at the surface.~~, High O₃ remained
37 ~~in the residual layer at night, and would and be then~~ transported to the surface by downward airflows
38 or turbulences ~~by the second day~~. Moreover, O₃ can be accumulated and trapped on the ground due
39 to the poor diffusion conditions because the vertical diffusion and horizontal diffusion were
40 suppressed by downward airflows and light wind, respectively. The premature mortalities attributed
41 to O₃ exposure in the YRD during the study period ~~was~~ 194.0, more than the casualties caused
42 directly by the typhoons. This work ~~has~~ enhanced our understanding of how landfall typhoons
43 affect O₃ in the YRD ~~and thus can be useful, which can be helpful~~ to forecast ~~the~~ O₃ pollution
44 ~~synthetically impacted by the subtropical high and typhoon~~ ~~in regions strongly influenced by~~
45 ~~typhoon activities.~~

46 **Key Words:** ozone; landfall typhoon; the Yangtze River Delta region;

47

48 1 Introduction

49 The tropospheric ozone (O₃), which is formed by a series of complex photochemical reactions
50 between volatile organic compounds (VOCs) and nitrogen oxides (NO_x=NO+NO₂) in combination
51 with sunlight (Chameides and Walker, 1973; Xie et al., 2014), has received continuous attention due
52 to its negative impact on air quality (Chan and Yao, 2008; Monks et al., 2015), human health (Jerrett
53 et al., 2009), climate (Allen et al., 2012; IPCC, 2014) and biosphere (Dingenen et al., 2009).
54 Research on urban O₃ pollution can ~~be dated~~ back to the early 1950s, beginning with the Los Angeles
55 smog. In China, the photochemical smog, which is characterized by high level of O₃, was first
56 discovered in Xigu district of Lanzhou in 1970s (Tang et al., 1989). However, with the key
57 atmospheric environmental problem was coal-smoke pollution (such as acid rain) at that time (Wang
58 et al., 2019), little systematic research and coordinated O₃ monitoring were performed in China until
59 the mid-2000s (Wang et al., 2017).

60 Since the beginning of ~~the~~ 21st century, the complex air pollution, which is dominated by fine

particulate matter (PM_{2.5}, particles of 2.5 microns or less in aerodynamic diameter) and surface O₃, has been ingrained in the megacities of China (Chan and Yao, 2008; Jin et al., 2016; Kan et al., 2012). Air pollution has evolved into a political and economic concern in China. Due to ~~the strict~~dratic air pollution control since 2013, particle pollution has been greatly reduced, appearing a significantly decrease in sulfur dioxide (SO₂), NO_x and PM_{2.5}. However, the concentrations of O₃ and VOCs ~~haved an~~ increased from 2013 to 2017 (Li et al., 2017), suggesting that more attention should be paid to controlling O₃ and VOCs in the future. Overall, the causes of air pollution ~~and the control policies in China~~ are ~~remaining still a major challenges to confront in China~~, especially in understanding the sources, transport and dispersion processes, and chemical formation mechanisms of O₃ and its precursors (Ding et al., 2016; Guo et al., 2014; Huang et al., 2014).

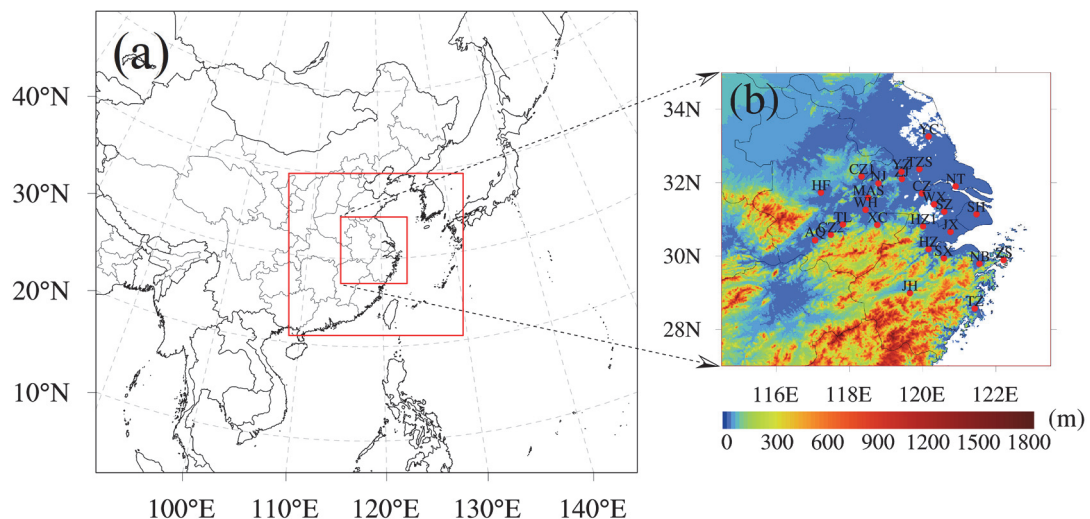
A typhoon (tropical cyclone, TC) is one of the most ~~severe important factors of~~ natural disasters in East Asia. Out of the total provinces in China, 10 coastal and 6 island provinces are affected by typhoon induced disasters, with more than 250 million lives are affected (Liu et al., 2009). The average number of typhoons making landfall in China is 9 each year, and those typhoons usually inflict vast losses in human life and property due to the accompanied strong wind, torrential rains and huge storm surges (Zhang et al., 2009; Zhao et al., 2012). Because of the long lifetime and tremendous energy, typhoons ~~can has a~~ significantly ~~impact influence on~~ local atmospheric conditions, and thereby can affect surface O₃ concentration through advection, diffusion, deposition and other processes. The impact of typhoons on O₃ has attracted extensive attention in recent years (Deng et al., 2019; Huang et al., 2005; Jiang et al., 2015; Shu et al., 2016; Wang and Kwok, 2002; Wei et al., 2016; Yang et al., 2012). For example, Deng et al. (2019) reported that high O₃ and high aerosol concentrations (double high episodes) are likely to occur when the PRD is under the control of ~~the~~ typhoon periphery and ~~the~~ subtropical high with strong downdrafts. Previous studies were mainly in the southern China (including Hong Kong and Taiwan), where ~~are frequently affected by~~ typhoons occur frequently. Still~~However~~, research on the impact of landfall typhoons on O₃ is ~~rather~~still limited.

The Yangtze River Delta (YRD) region, being one of the most developed and densely populated regions in China, is located on the western coast of the Pacific Ocean. With 3.7% of the area and 16.0% of the population of China, the YRD contributed over 20% of the national total Gross Domestic Product (GDP) in 2019. Due to the rapid economic development and high energy

91 consumption, this region ~~has been~~ suffering from intense air pollution (Ding et al., 2013; Li et al.,
92 2019; Wang et al., 2015; Xie et al., 2016). In 2017, the 90th percentile of the maximum daily 8-hour
93 average (MDA8) O₃ concentration was 170 μg m⁻³, and 16 of the 26 cities (Figure 1b) in the YRD
94 failed to meet national standard (http://www.cnemc.cn/jcbg/zghjzkgb/201905/t20190529_704755.html). Therefore, it is ~~an~~ urgent ~~task~~ to investigate the spatiotemporal characteristic of O₃ as well as
95 its formation mechanisms ~~s~~ in the YRD. Influenced by ~~the~~ monsoon weather, the warm and stagnation
96 conditions play an important role in the occurrence of high-level O₃ in summer (Li et al., 2018; Liao
97 et al., 2015; Lu et al., 2018; Zhao et al., 2010). Synoptic weather systems, such as typhoons ~~s~~ and
98 cold fronts, ~~can also have~~ significantly ~~impact effects on~~ O₃ in the YRD (Hu et al., 2013; Shu et al.,
99 2016). This work aims to reveal the main processes of landfall typhoon affecting surface O₃ in the
100 YRD, ~~hoping~~ to fill the knowledge gap and ~~thus provide scientific insight be helpful~~ for
101 ~~effectivemaking reasonable~~ pollution control measures.

103 In this study, we report a ~~typicaln outstanding~~ case observed in the YRD during the period from
104 16 July to 25 August, ~~2018,~~ during which multiday episode of high O₃ occurred and was ~~found to~~
105 ~~be~~ related to four successive landfall typhoons. Base on the monitoring data and numerical
106 simulation, we ~~further~~ explore the impact of landfall typhoons on O₃ in the YRD, including the
107 major processes and health impacts. The following part of this paper is structured as the follows:
108 Section 2 gives a brief description of monitoring data, the analysis methods, and model
109 configurations. The results as well as the discussions are detailed in section 3. Section 4 summarizes
110 the main conclusions.

111



112
113 **Figure 1.** The three nested modeling domains (a) in WRF, and the locations of 26 typical cities
114 in the YRD with terrain elevation data (b). The cities in (b) include: Nanjing (NJ), Wuxi (WX),
115 Changzhou (CZ), Suzhou (SZ), Nantong (NT), Yancheng (YC), Yangzhou (YZ), Zhenjiang (ZJ)
116 and Taizhou (TZS) located in Jiangsu province; Hangzhou (HZ), Ningbo (NB), Jiaxing (JX),
117 Huzhou (HZ1), Shaoxing (SX), Jinhua (JH), Zhoushan (ZS) and Taizhou (TZ) located in
118 Zhejiang province; Hefei (HF), Wuhu (WH), Maanshan (MAS), Tongling (TL), Anqing (AQ),
119 Chuzhou (CZ1), Chizhou (CZ2) and Xuancheng (XC) located in Anhui province; and the
120 megacity Shanghai (SH). The terrain elevation data are available at
121 https://www.ngdc.noaa.gov/mgg/global/relief/ETOPO1/data/bedrock/cell_registered/netcdf/.
122

123 2 Data and methods

124 2.1 Air quality data

125 Surface air pollutants monitored by the China National Environmental Monitoring Center
126 (CNEMC) Network are used in this study. The nationwide observation network began operating in
127 74 major cities in 2013, and it included 1597 nonrural sites covering 454 cities by 2017 (Lu et al.,
128 2018). The monitoring data are strictly in accordance with the national monitoring regulations
129 (<http://www.cnemc.cn/jcgf/dqhj/>), and can be acquired from the national urban air quality real-time
130 publishing platform (<http://106.37.208.233:20035/>). Each monitoring site automatically measures
131 hourly air pollutants (PM_{2.5}, PM₁₀, SO₂, NO₂, O₃ and CO), and the urban hourly pollutants are
132 calculated by averaging the pollutants measured at all monitoring sites in that city. The MDA8 O₃

133 is calculated based on the hourly O₃ with more than 18-h measurements (Liao et al., 2017). Manual
134 inspection, including the identification and handling of invalid and lacking data, is performed
135 following previous studies (Xie et al., 2016; Shu et al., 2017; Zhan et al., 2019).

136 **2.2 Surface and sounding meteorological data**

137 With respect to surface observed meteorological data, stations at the three provincial capital
138 cities (Hefei, Nanjing and, Hangzhou and Hefei) and the megacity Shanghai are selected, which
139 are ZSOF (117.23°E, 31.87°N), ZSNJ (32.00°N, 118.80°E, 32.00°N), ZSHC (30.23°N, 120.17°E,
140 30.23°N), ZSOF (31.87°N, 117.23°E) and ZSPD (31.12°N, 121.77°E, 31.12°N), respectively. These
141 surface observations, including 2-m temperature, 10-m wind speed and direction and 2-m relative
142 humidity, are recorded hourly and can be obtained from the website of the University of Wyoming
143 (<http://weather.uwyo.edu/surface/>). The precipitation data is not included in the dataset.

144 To verify the upper-air fields, the sounding observations at Shanghai (31.40°N, 121.46°E,
145 31.40°N) and Nanjing (32.00°N, 118.80°E, 32.00°N) are used. These sounding observations
146 (pressure, temperature, relative humidity, wind direction and wind speed etc.) are also acquired from
147 the website of the University of Wyoming (<http://weather.uwyo.edu/upperair/sounding.html>), with
148 a time resolution of 12 h (00:00 and 12:00 UTC).

149 **2.3 The best-track TC dataset**

150 To capture the characteristics of landfall typhoons, the best-track TC dataset issued by the
151 China Meteorological Center (CMA) is considered due to its good performance on the landfall
152 typhoons in the mainland China (available at http://tcdatalyphoon.org.cn/zjljsjj_sm.html). The
153 dataset covers seasons from 1949 to the present, the region north of the equator and west of 180°E,
154 and is updated annually (Li and Hong, 2016; Ying et al., 2014). A wealth of information on typhoon
155 is recorded every 6h in the dataset, including location, minimum sea level pressure, etc. For landfall
156 typhoons, 24h before their landing on land and during their activities in the mainland China, the
157 meteorological data are will be recorded every 3h. Refer to the national standard for grade of tropical
158 cyclones (GB/T 19201-2006), the intensity category (IC) of tropical cyclones is provided given in
159 the dataset, which is based on the near surface maximum 2-min mean wind speed near the tropical
160 cyclone center, ranging from 1 to 6 (Table 1).

161

162 **Table 1. The intensity category of tropical cyclones**

Intensity category (IC)	The near surface maximum 2-min mean wind speed near the tropical cyclone center (m/s)	Beaufort scale
Tropical depression (IC=1)	10.8-17.1	6-7
Tropical storm (IC=2)	17.2-24.4	8-9
Severe tropical storm (IC=3)	24.5-32.6	10-11
Typhoon (IC=4)	32.7-41.4	12-13
Severe typhoon (IC=5)	41.5-50.9	14-15
Super typhoon (IC=6)	≥ 51.0	≥ 16

163

164 **2.4 Model description and configurations**

165 To simulate the high O₃ episodes over the YRD during the ~~period with typhoon~~periods, the
 166 WRF-CMAQ one-way coupled model is applied, which consists of WRF v3.6.1
 167 (<https://www2.mmm.ucar.edu/wrf/users/>) developed by the United States National Center for
 168 Atmospheric Research (NCAR) and CMAQ v5.0.2 (<https://github.com/USEPA/CMAQ/tree/5.0.2>)
 169 developed by the United States Environmental Protection Agency (EPA).

170 WRF generates offline meteorological inputs for CMAQ with initial and boundary conditions
 171 from the National Centers for Environmental Prediction (NCEP) global final analysis fields every
 172 6 h at a spatial resolution of 1° × 1° (<https://rda.ucar.edu/datasets/ds083.2/>). Three nested domains
 173 are used, with horizontal resolutions of 81, 27 and 9 km, and grids of 88 × 75, 85 × 79 and 97 × 97,
 174 respectively (Figure 1a). There are 24 vertical sigma layers from surface to 100 hPa, with about 8
 175 layers located below 1.5 km to resolve the boundary layer processes. Furthermore, the major
 176 physical options for the dynamic parameterization in WRF are summarized in Table 2.

177

178 **Table 2. The domains and physical options for WRF in this study**

Items	Contents
Dimensions (x, y)	(88, 75), (85, 79), (97, 97)
Grid spacing (km)	81, 27, 9
Microphysics	WRF Single-Moment 5-class scheme (Hong et al., 2004)
Longwave radiation	RRTM scheme (Mlawer et al., 1997)

Shortwave radiation	Goddard scheme (Kim and Wang, 2011)
Surface layer	Moni-Obukhov scheme (Monin and Obukhov, 1954)
Land-surface layer	Noah land-surface model (Chen and Dudhia, 2001)
Planetary boundary layer	YSU scheme (Hong et al., 2006)
Cumulus parameterization	Grell-Devenyi ensemble scheme (Grell and Devenyi, 2002)

179

180 Since the horizontal domains of CMAQ are one grid smaller than WRF, all three nested
 181 domains are adjusted automatically. The vertical layers of CMAQ are the same as WRF. The
 182 Meteorology Chemistry Interface Processor (MCIP) can convert WRF outputs to the necessary
 183 meteorological inputs for CMAQ. Moreover, the CB05 gas-phase mechanism with aqueous/cloud
 184 chemistry is selected in the CMAQ configurations.

185 The anthropogenic emissions are from the Multi-resolution Emission Inventory for China
 186 (MEIC) in 2016 with the resolution of 0.25° (<http://meicmodel.org/>), including anthropogenic
 187 emissions from power generation, industry, agriculture, residential and transportation sectors. All
 188 emission estimates are spatially allocated to the relevant grid cells based on the meteorological fields
 189 obtained from WRF, and are temporally distributed on an hourly basis. The simulation starts from
 190 00:00 UTC on 13 July to 00:00 UTC 27 August, with the first 72 h as spin-up time.

191 **2.5 Integrated process rate (IPR) analysis**

192 To quantify the contributions of individual processes ~~to~~ O_3 formation, the IPR analysis
 193 provided in the CMAQ is utilized. The IPR analysis can illustrate the contributions to changes in
 194 pollutant concentrations from seven different types of processes, including horizontal advection
 195 (HADV), vertical advection (ZADV), horizontal diffusion (HDIF), vertical diffusion (VDIF), dry
 196 deposition (DDEP), cloud processes with the aqueous chemistry (CLDS) and chemical reaction
 197 process (CHEM), with a mass conservation adjustment at each model grid cell. The IPR analysis
 198 has been widely applied to investigate regional air pollution (Fan et al., 2015; Li et al., 2012; Wang
 199 et al., 2010). In this study, MADV is defined as the sum of HADV and ZADV, and TDIF is defined
 200 as the sum of HDIF and VDIF.

201 **2.6 Model evaluation**

202 To evaluate the model performance, the simulation results in the innermost domain, including
 203 O_3 concentration, air temperature at 2 m (T_2), relative humidity (RH), wind speed at 10 m (WS_{10})

204 and wind direction at 10 m (WD_{10}), are examined against the hourly observations at the
 205 representative cities (Table 3). The statistical metrics, including correlation coefficient (R), root-
 206 mean-square error (RMSE) and normalized mean bias (NMB), are used ~~in this study~~. They are
 207 defined as follows:

$$208 R = \frac{\sum_{i=1}^N (S_i - \bar{S})(O_i - \bar{O})}{\sqrt{\sum_{i=1}^N (S_i - \bar{S})^2} \sqrt{\sum_{i=1}^N (O_i - \bar{O})^2}}, \quad (3)$$

$$209 RMSE = \sqrt{\frac{\sum_{i=1}^N (S_i - O_i)^2}{N}}, \quad (4)$$

$$210 NMB = \frac{\sum_{i=1}^N (S_i - O_i)}{\sum_{i=1}^N O_i} \times 100\%, \quad (5)$$

211 where S_i and O_i are the simulations and observations, respectively. N is the total number of valid
 212 data. \bar{S} and \bar{O} are the average value of simulations and observations, respectively. In general, the
 213 model results are acceptable if the values of R, RMSE and NMB are close to 1, 0 and 0, respectively
 214 (Li et al., 2017; Shu et al., 2016; Xie et al., 2016).

215 2.7 Estimate of health impacts

216 Previous studies showed that surface O_3 pollution can induce a series of adverse health
 217 problems impacts by causing from the incidence and mortality of respiratory diseases (Ghude et al.,
 218 2016; Jerrett et al., 2009; Lelieveld et al., 2015). To arouse more attention on the issue that O_3 can
 219 be significantly affected by typhoons in the YRD, we further estimate the premature mortality
 220 attributed to O_3 during the study period.

221 A standard damage function (Anenverg et al., 2010; Liu et al., 2018; Voorhees et al., 2014;
 222 WS/T 666-2019, Technical specifications for health risk assessment of ambient air pollution of
 223 China) is employed to quantify premature mortality due to O_3 exposure:

$$224 \Delta M = y_0 \left(\frac{RR - 1}{RR} \right) Pop, \quad (1)$$

225 where ΔM is the excess mortalities attribute to O_3 exposure, y_0 is the baseline mortality rate, RR is
 226 relative risk and $(RR-1)/RR$ is the attributable fraction, and Pop is the exposed population. RR can

227 be calculated using the following relationship:

228
$$RR = \exp(\beta(C - C_0)), \quad (2)$$

229 where β is the concentration-response factor, C is the exposure concentration and C_0 represents the
230 theoretical minimum-risk concentration.

231 In this study, the mortality rate for respiratory disease is obtained from China Health and
232 Family Planning Statistical Yearbook 2018 (<https://www.yearbookchina.com/navibooklist-n3018112802-1.html>), which is 68.02/100000. The β is generated from Dong et al. (2016), that is
233 0.461%. The population data are obtained from the Bureau of Statistics of different cities in the
234 YRD. The C_0 is $70 \mu\text{g m}^{-3}$ for MDA8 O₃ given by the World Health Organization (WHO).

235

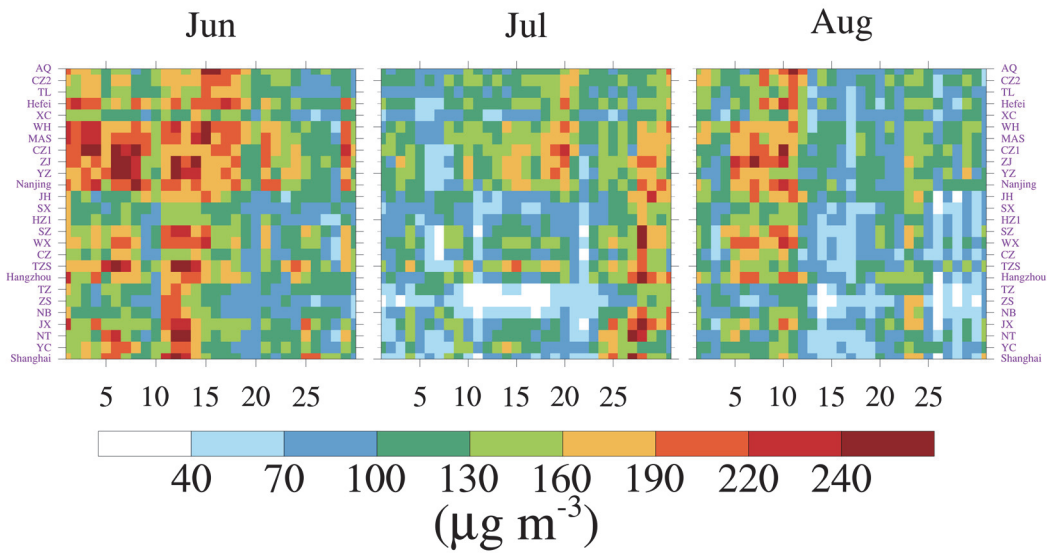
236

237 **3 Results and discussions**

238 **3.1 Characteristic of O₃ episodes**

239 In the midsummer—~~season~~, the warm sea surface (high temperature) is conducive to the
240 generation of typhoons~~s~~ (high O₃ concentration),~~which providing~~ a good opportunity to investigate
241 the mechanism of typhoons~~s~~ affecting O₃ in the YRD. Figure 2 shows the MDA8 O₃ in the typical
242 26 cities of the YRD in summer of 2018.~~Actually, it is common for typhoons to affect O₃ in the~~
243 ~~YRD during summer, and 2018 is special because there were 8 landfall typhoons and many of them~~
244 ~~landed further north than in the normal years (see Supplement for details)~~. O₃ concentration ~~was~~
245 ~~relatively tended to be~~ high in June, and relatively low in July and August. The relatively low O₃
246 may be attributed to the maritime air masses transported by the Asian summer monsoon (Ding et
247 al., 2008; Xu et al., 2008). Nevertheless, we notice that there are two regional multiday O₃ pollution
248 episodes from 24 July to 11 August in the YRD, which means that about half of the cities in the
249 YRD exceed the national air quality standard (The national ambient air quality standard for MDA8
250 O₃ is $160 \mu\text{g m}^{-3}$ in China). The first multiday O₃ episodes appeared in most ~~of the~~ cities from 24
251 July to 2 August. The highest MDA8 O₃ concentration reached up to $264 \mu\text{g m}^{-3}$ on 27 July in
252 Ningbo (NB). O₃ pollution was even observed for 6 consecutive days from 27 July to 1 August in
253 Maanshan (MAS). Only two days later, regional O₃ pollution occurred in the YRD again from 5
254 August to 11 August.

255

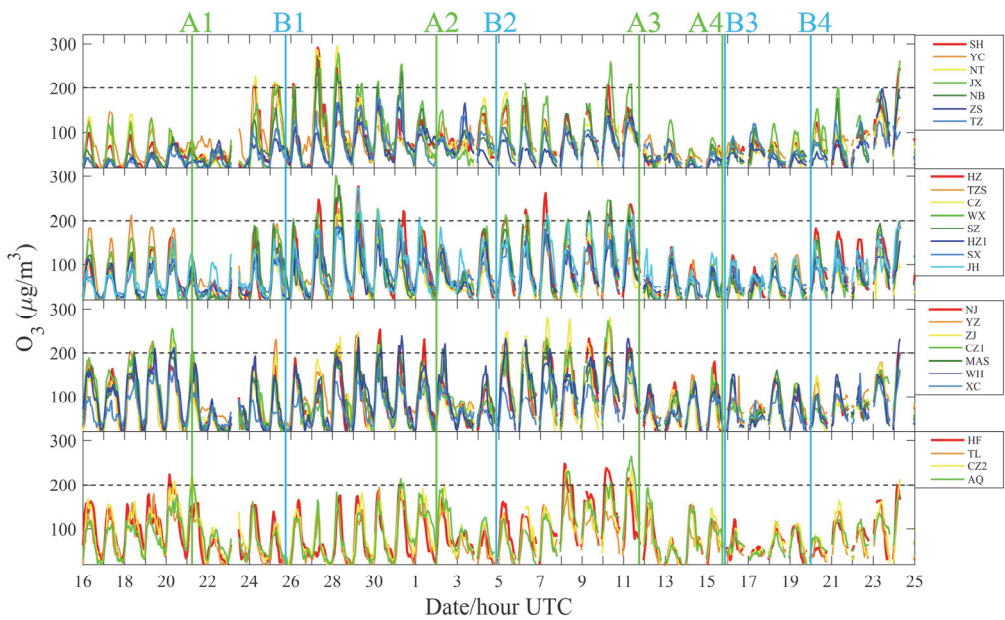


256
257 **Figure 2. The MDA8 O₃ in 26 cities of the YRD in June (left panel), July (middle panel), and**
258 **August (right panel) 2018 summer of 2018.** The national ambient air quality standard for
259 MDA8 O₃ is 160 $\mu\text{g m}^{-3}$ in China. These cities are sorted by longitude.
260

261 Figure 3 further shows diurnal variation of O₃ in all 26 cities of the YRD from 00:00 16 July
262 to 00:00 25 August (throughout this paper the time refers to UTC, unless LST is specifically
263 stated mentioned). Interestingly, O₃ pollution occurred earlier in cities near the coastline (e.g. large
264 longitudes in °E, Figure 1b) rather than concurrently during the two multiday O₃ episodes. For
265 example, from 24 July to 2 August, the first day that hourly O₃ concentration exceeded the national
266 air quality standard (The national ambient air quality standard for hourly O₃ is 200 $\mu\text{g m}^{-3}$ in China)
267 in Shanghai, Hangzhou, Nanjing and Hefei was 24 July, 27 July, 28 July and 31 July, respectively.
268 Thus, we classify the 26 cities in the YRD into four categories based on their longitudes, surrounding
269 the four representative cities (Figure 4). The category I cities include SH, YC, NT, JX, NB, ZS and
270 TZ. The category II cities include HZ, TZS, CZ, WX, SZ, HZ1, SX and JH, and the category III
271 cities include NJ, YZ, ZJ, CZ1, MAS, WH and XC. Other cities are classified as the category IV
272 cities, which are HF, TL, CZ2 and AQ. The first category cities are closest to the coastline, while
273 the fourth category is the opposite.

274

275



276

Figure 3. Diurnal variation of O₃ in all 26 cities of the YRD from 16 June to 25 August, 2018.

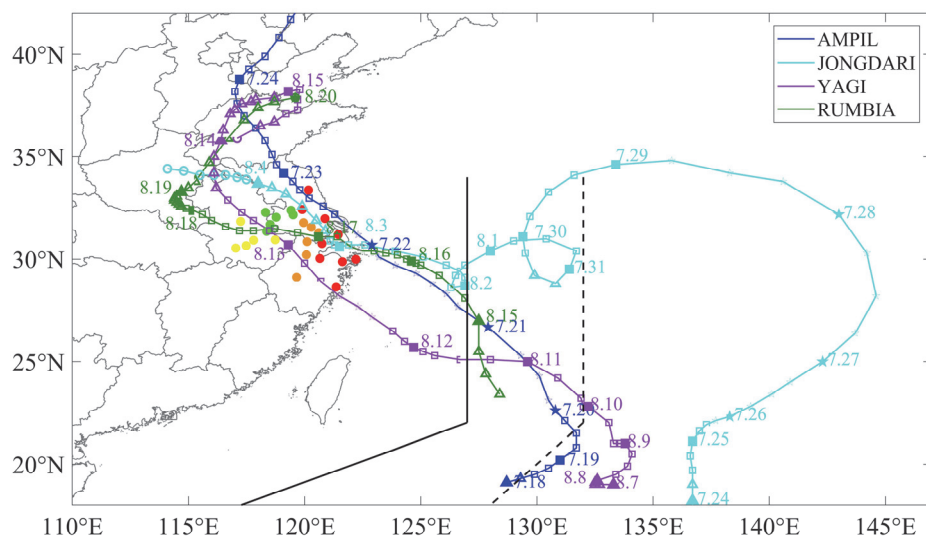
The grey dotted lines are the national ambient air quality standard for hourly O₃ (200 $\mu\text{g m}^{-3}$) in China. The letter A indicates the moment that the typhoon has reached the 24-h warning line, and letter B indicates the last moment when the typhoon was active in the mainland China. These time moments are acquired from the best-track TC dataset, depending on the start and end times of the 3h densified observations. Coordinates 1, 2, 3, and 4 represent Typhoon Ampil, Typhoon Jongdari, Typhoon Yagi, and Typhoon Rumbia, respectively. Note: these cities are sorted by longitude.

285

286 **3.2 Landfall typhoons and their effects**

287 For such O₃ episodes with regional and, long-lasting characteristics, may often be associated
 288 with slow-moving synoptic weather systems. We find that the O₃ episodes coincided well with
 289 activities of landfall typhoons activities, showing in their and the tracks and intensities of typhoons
 290 are given in Figure 4. Typhoon Ampil was first observed at 00:00 on 18 July, and landed in Shanghai
 291 around 4:30 on 22 July with an intensity of severe tropical storm (IC=3). While During the time of
 292 Typhoon Ampil remained active, Typhoon Jongdari generated over the western North Pacific at
 293 12:00 on 23 July, and made landfall at the junction of Zhejiang province and Shanghai at 21:00 1
 294 August. After Typhoon Jongdari, Typhoon Yagi generated at 00:00 7 August. At around 15:35 12
 295 August, it landed in Zhejiang province and remained active in the mainland China until 21:00 15
 296 August. Before the end of Typhoon Yagi, Typhoon Rumbia was observed over the western North
 297 Pacific at 6:00 14 August. It finally landed in Shanghai at around 20:00 16 August, causing huge
 298 economic losses.

299



300

301 **Figure 4. The track and intensity of Typhoon Ampil, Typhoon Jongdari, Typhoon Yagi, and**
 302 **Typhoon Rumbia. The track is labeled with the date of the month and day (in month.day).**
 303 The circle, triangle, square and pentagram indicate the intensity category of tropical cyclones
 304 is less than 1 (IC < 1), equal to 1 (IC = 1), equal to 2 (IC = 2), and not less than 3 (IC ≥ 3),
 305 respectively. Black solid line and dotted line represent the 24-hour and 48-h warning line for

306 tropical cyclones, respectively. The colored solid points are the locations of cities in the YRD,
307 and different color represents different cities categories. Wherein, red, carrot, green and
308 yellow are category I, II, III and IV cities, respectively.

309

310 To further understand the relationship between O₃ episodes and landfall typhoons, we mark the
311 critical moments of landfall typhoons in Figure 3. The letter A indicates the moment when at that
312 typhoons hasve reached the 24-h warning line, and the letter B indicates the last moment of that
313 typhoon remains activeactivity in the mainland China. These moments are acquired from the best-
314 track TC dataset, depending on the start and the end time of the densified-3h observations.
315 Coordinates 1, 2, 3, and 4 represent Typhoon Ampil, Typhoon Jongdari, Typhoon Yagi, and Typhoon
316 Rumbia, respectively. As shown in Figure 3, O₃ exhibited a significant cycle during the study period.
317 That is, when the typhoon is close enough (near moments A1, A2, A3 and A4), the O₃ concentrations
318 decreased, but O₃ concentrations would increase as long as the typhoon was not active in the
319 mainland China (B1, B2 and B4) any more. This cycle would repeat if the next typhoon approached.
320 O₃ pollution was likely to occur during the period from the end of at the typhoon to the arrival of the
321 next typhoon (B1A2 and B2A3) in the YRD.

322 Furthermore, we find that the variations of O₃ was related to the track, duration and landing
323 intensity of the typhoons. For example, during the B1A2 period when the O₃ pollution occurred, the
324 moments that hourly O₃ concentrations first exceed 200 $\mu\text{g m}^{-3}$ in about half of cities of the
325 categories I, II, III and IV were 6:00 UTC (14:00 LST) 27 July, 6:00 UTC (14:00 LST) 28 July, 3:00
326 UTC (11:00 LST) 29 July and 6:00 UTC (14:00 LST) 31 July, respectively. This phenomenon also
327 suggests that O₃ pollution first occurs- in cities along the coastlinein coastal region will be ahead
328 of that in inland regions, which may be related to the track of typhoons (Figure 4). RegardingAs for
329 the impact of typhoon duration, the A4B3 period provided a good interpretation. While Typhoon
330 Yagi was still active in the mainland China, Typhoon Rumbia had reached the 24-hour warning line.
331 Hence, the O₃ remained a low level throughout the period (A3B4), which was quite different from
332 B1A2 and B2A3 period. Noted that the landing point and active path of Typhoon Ampil and
333 Typhoon Jongdari were very similar (Figure 4). However, the landing intensity of Typhoon Ampil
334 was severe tropical storm (IC = 3), and that of Typhoon Jongdari was tropical storm (IC = 2),
335 resulting in a difference in O₃ concentrations for Shanghai. Within 24 hours after Typhoon Ampil

336 (Jongdari) reached the 24-hour warning line, the average O₃ concentrations ~~reached was~~ 40.9 (80.1)
337 µg m⁻³ in Shanghai. This is because that the stronger the typhoon landed, the gale (The 10-m wind
338 speed near moment A1 was larger than that near moment A2 in Shanghai, Figure 7a) and
339 precipitation accompanying the typhoon will be more effective in removing O₃.

340 **3.3 Processes of O₃ pollution affecting by typhoons**

341 To reveal the major processes of O₃ pollution episodes affected by landfall typhoons, ~~four~~
342 ~~representative cities (Shanghai, Hangzhou, Nanjing and Hefei)~~ one municipality and three provincial
343 capital cities with different longitudes, including Shanghai (121.77°E, 31.12°N), Hangzhou
344 (120.17°E, 30.23°N), Nanjing (118.80°E, 32.00°N) and Hefei (117.23°E, 31.87°N), are selected for
345 further analysis – based on monitoring data and model results.

346 **3.3.1 Evaluation of model performance**

347 To evaluate the simulation performance, the hourly simulation results are compared with the
348 measurements ~~from~~~~during~~ 00:00 16 July to 00:00 25 August. Table 3 presents the statistical metrics
349 for selected variables, including temperature at 2 m (T₂), relative humidity (RH), wind speed at 10
350 m (WS₁₀)~~, and~~ wind direction at 10 m (WD₁₀), and surface O₃. T₂ is reasonably well simulated, with
351 R values of 0.75, 0.77, 0.72 and 0.64 in Shanghai, Hangzhou, Nanjing and Hefei, respectively.
352 Though our simulation underestimates T₂ to some ~~certain~~ extent, ~~this~~ slightly underestimation is
353 acceptable ~~because of~~~~due to~~ the small RMSE (3.2, 2.7, 2.9 and 3.3) and NMB (-7.5%, -5.1%, -5.5%
354 and -5.5%) values. As for RH, the simulation results are overestimated in all four cities, leading to
355 the NMB values of 9.1%, 4.6%, 6.7% and 0.5% in Shanghai, Hangzhou, Nanjing and Hefei,
356 respectively. With high R values (0.69, 0.65, 0.71 and 0.71) and relatively low RMSE values (12.4,
357 12.8, 12.1 and 10.8), the WRF simulates RH over the YRD quite well. The wind fields are closely
358 related to the transport processes of air pollutants. The overestimation of WS₁₀ may partly be
359 attributed to the unresolved terrain features by the default surface drag parameterization causing
360 overestimation of wind speed in particular at low values (Jimenez and Dudhia, 2012; Li et al., 2017).
361 With regards to WD₁₀, the simulation error is large based only on these statistical metrics. This is
362 because that near-surface wind fields are deeply influenced by local underlying surface
363 characteristics, and improving the urban canopy parameters might be useful (Liao et al., 2015; Xie
364 et al., 2016). In term of O₃, the simulated ~~edition~~ results for O₃ concentrations behave satisfactorily. R
365 is ~~as high as~~ 0.55, 0.65, 0.66 and 0.54 ~~for the simulations for~~ in Shanghai, Hangzhou, Nanjing and

366 Hefei, respectively, while the NMB values are 5.8%, 16.4%, -6.2% and -5.3%, respectively.

367

368 **Table 3. Statistical metrics infor meteorological variables and O₃ concentration between the**
369 **observations and simulationshemeical variables.**

City	Variable	\bar{O}	\bar{S}	R	RMSE	NMB
Shanghai	T ₂ (°C)	30.3	28.1	0.75	3.2	-7.5%
	RH (%)	75.0	81.8	0.69	12.4	9.1%
	WS ₁₀ (m s ⁻¹)	4.9	5.5	0.51	2.3	11.7%
	WD ₁₀ (°)	144.8	113.4	0.01	113.5	-22.9%
	O ₃ (μg m ⁻³)	74.3	76.5	0.55	45.3	5.8%
Hangzhou	T ₂ (°C)	30.3	28.8	0.77	2.7	-5.1%
	RH (%)	75.1	78.5	0.65	12.8	4.6%
	WS ₁₀ (m s ⁻¹)	3.3	4.7	0.32	2.7	32.5%
	WD ₁₀ (°)	155.0	114.7	-0.10	132.5	-27.8%
	O ₃ (μg m ⁻³)	81.7	91.3	0.65	49.8	16.4%
Nanjing	T ₂ (°C)	29.8	28.1	0.72	2.9	-5.5%
	RH (%)	77.4	82.6	0.71	12.1	6.7%
	WS ₁₀ (m s ⁻¹)	3.1	5.0	0.39	3.0	63.8%
	WD ₁₀ (°)	132.8	115.6	0.21	102.7	-15.0%
	O ₃ (μg m ⁻³)	87.6	79.8	0.66	46.7	-6.2%
Hefei	T ₂ (°C)	29.3	27.7	0.64	3.3	-5.5%
	RH (%)	81.1	81.5	0.71	10.8	0.5%
	WS ₁₀ (m s ⁻¹)	3.2	3.2	0.37	2.2	2.9%
	WD ₁₀ (°)	147.0	128.6	0.04	136.7	-13.3%
	O ₃ (μg m ⁻³)	87.3	80.3	0.54	45.0	-5.3%

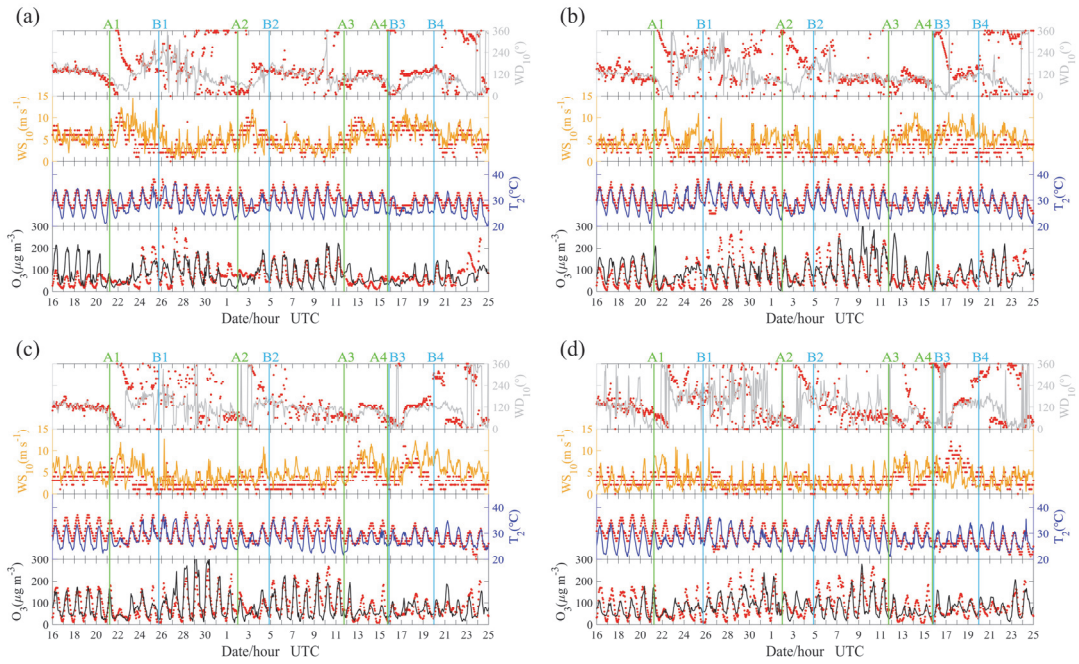
370 Note. R exceeds 0.1 to reach statistically significant at 99.9% confident level.- \bar{O} and \bar{S} are the
371 average values of the observations and simulations, respectively.

372

373 Figure 5 further shows hourly variations of O₃, T₂, WS₁₀ and WD₁₀ for measurements and
374 simulations in four representative cities. The simulations effectively reproduce the diurnal variation
375 of O₃, T₂ and WS₁₀, confirming the reliability of the simulation results. Moreover, the model well
376 captures the shift in wind direction during the study period. Thus, the overall model performance in
377 simulatingfor wind fields is acceptable. In summary, the simulationsresults can capture and
378 reproduce the major meteorological characteristics and O₃ evolution duringof the O₃ episodes, and
379 thusincluding the meteorological conditions and evolution of O₃, which can provide valuable

380 insights into the formation of the O₃ episodes.

381



382

383
384 **Figure 5. Hourly variations of O₃, T₂, WS₁₀ and WD₁₀ ~~infor~~ measurements (red dots) and**

385 simulation (colored lines) in (a) Shanghai, (b) Hangzhou, (c) Nanjing and (d) Hefei.

386

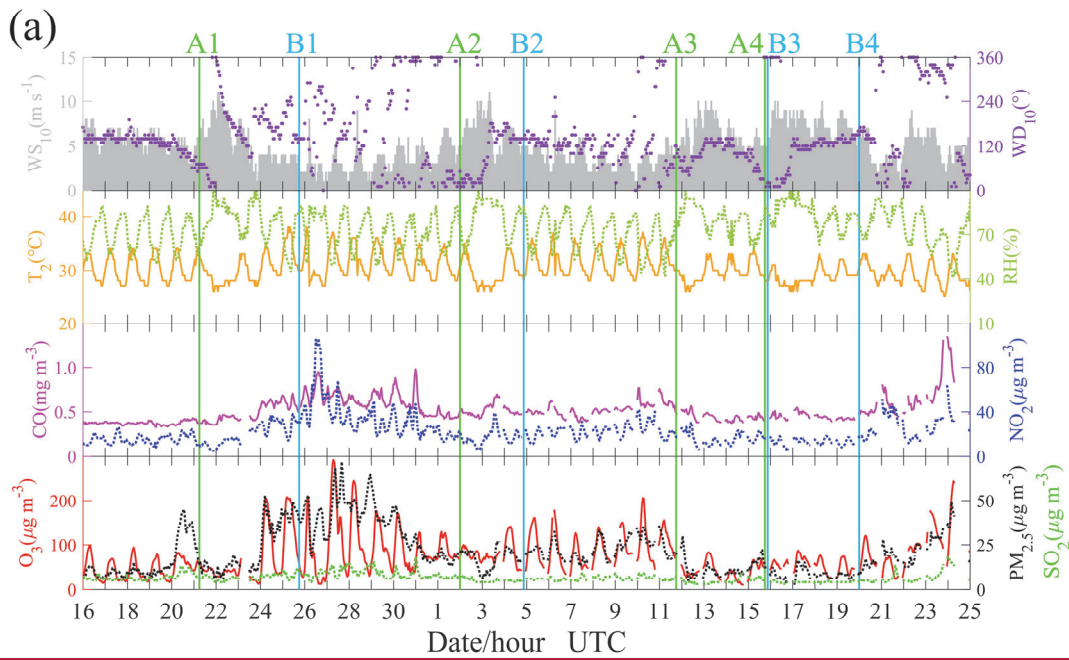
387 3.3.2 Shanghai in category I cities

388 In ~~this~~ study period, Shanghai was usually one of the first cities affected by landfall typhoons.
389 We can see a multiday episode of O₃ during the period of 24-28 July, with a maximum of hourly O₃
390 up to 292 µg m⁻³ at 27 July (Figure 6a). The high O₃ concentrations together with high primary
391 pollutants (CO and NO₂) suggest a strong photochemical O₃ production under the condition of high
392 temperature (The daily maximum temperature can reach 35 °C) during this period, and the weak
393 wind may play a significant role in the accumulation of surface O₃. The increase of the primary
394 pollutants may be related to the wind shifts a change in wind direction from southeast to southwest
395 causing by Typhoon Ampil (A1 in Figure 6a, -A1 and A1B1 in Figure 7), resulting in air masses
396 originally from the ocean had become inland which originally brought airmass from the ocean,
397 shifted to from inland. Interestingly, PM_{2.5} also showed good correlation with O₃ and primary
398 pollutants, especially for NO₂ during this period. This indicates that a high level of oxidizability can
399 promote the formation of secondary particles (Kamens et al., 1999; Khoder, 2002). From the results
400 of process analysis (Figure 6b), the major contributions to surface O₃ were TDIF, CHEM and DDEP

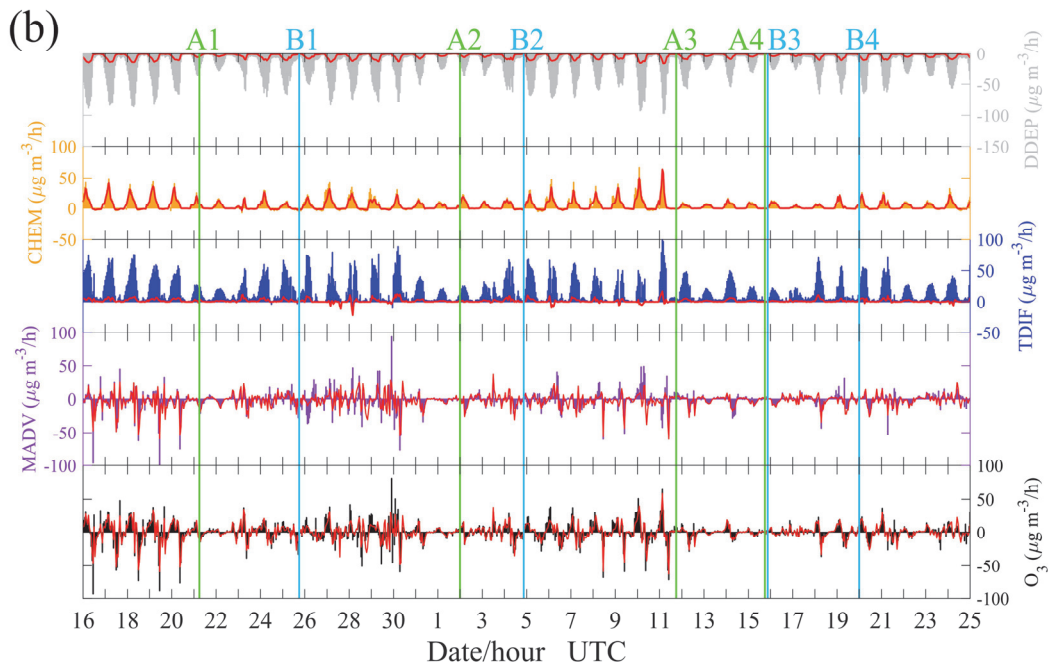
401 due to the small net contribution of MADV. TDIF had a considerable positive contribution while
402 DDEP did the opposite, suggesting that high surface O₃ may be sourced from the upper layer via
403 TDIF process, and be removed via DDEP process. However, for the whole boundary layer, which
404 is defined as the layer less than 1500 m in this study, ~~it was~~ the balance was between CHEM and
405 DDEP instead TDIF and DDEP. Thus, TDIF was likely to play the role of “transport” from the upper
406 layer to surface. Figure 6c further shows the temporal-vertical distribution of O₃ with vertical wind
407 velocity. The downward airflows ~~were~~ prevailed over Shanghai until 23 July, which are induced by
408 the subtropical high. Then, strong upward airflows appeared as Typhoon Ampil arrived, and high
409 level of O₃ disappeared. Around 27 July, the downward airflows gradually resumed and high level
410 of O₃ occurred. The downward airflows are critical because they can not only inhibit the vertical
411 transport of O₃ but also transport high-level O₃ to the surface. The high-level O₃ in the troposphere
412 mainly comes from two sources. One is that O₃-rich air from the low stratosphere transported by
413 the downdrafts in large-scale typhoon circulation (Jiang et al., 2015). The other is that O₃ produced
414 by photochemical reactions during the day. It is note-worthy that ~~the high value center of O₃~~
415 ~~appeared near the altitude of 1 km instead of near surface, indicating high photochemical production~~
416 efficiency of O₃ occurred in the middle boundary layer instead of at the surface. Moreover, most of
417 the O₃ remained in the residual layer at night, while surface O₃ concentration was much lower due
418 to NO_x titration. By the second day, high O₃ in the residual layer was transported to the surface by
419 the downward airflows as air in the boundary layer is gradually mixed. Combined with the newly
420 generated O₃, a high concentration of O₃ would eventually appear on the surface. –The downward
421 airflows can not only inhibit the vertical transport of O₃ but also transport high-level O₃ to the
422 surface, causing the episodes of surface O₃.

423 As shown in Figure 7, O₃ pollution tends to occur during the period from the end of ~~at the~~
424 typhoon to the arrival of the next typhoon (B1A2 and B2A3) in the YRD. To reveal this phenomenon,
425 we compare these two periods (B1A2 and B2A3) with their previous periods (A1B1 and A2B2)
426 using the skew-T log-P diagram (Figure 6d and 6e). It is found that the atmospheric conditions of
427 B1A2 (B2A3) were hotter and drier than A1B1 (A2B2) below 700 hPa in Shanghai, and wind speed
428 is smaller in B1A2 (B2A3). Those changes in atmospheric conditions after typhoon will be
429 conducive to the generation of high O₃ concentration in Shanghai.

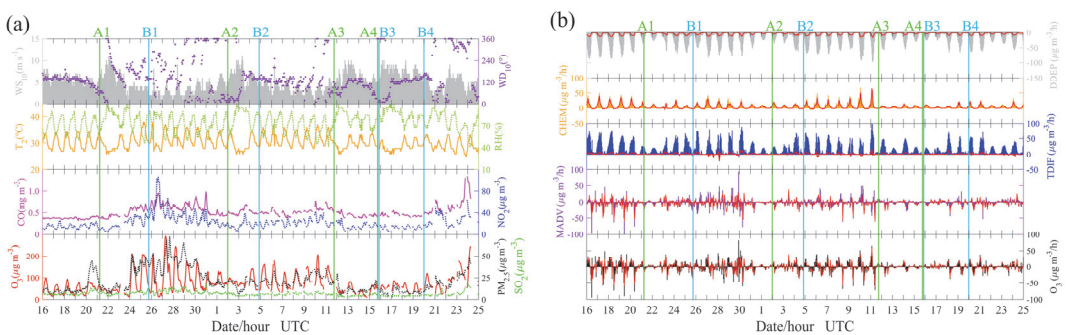
431

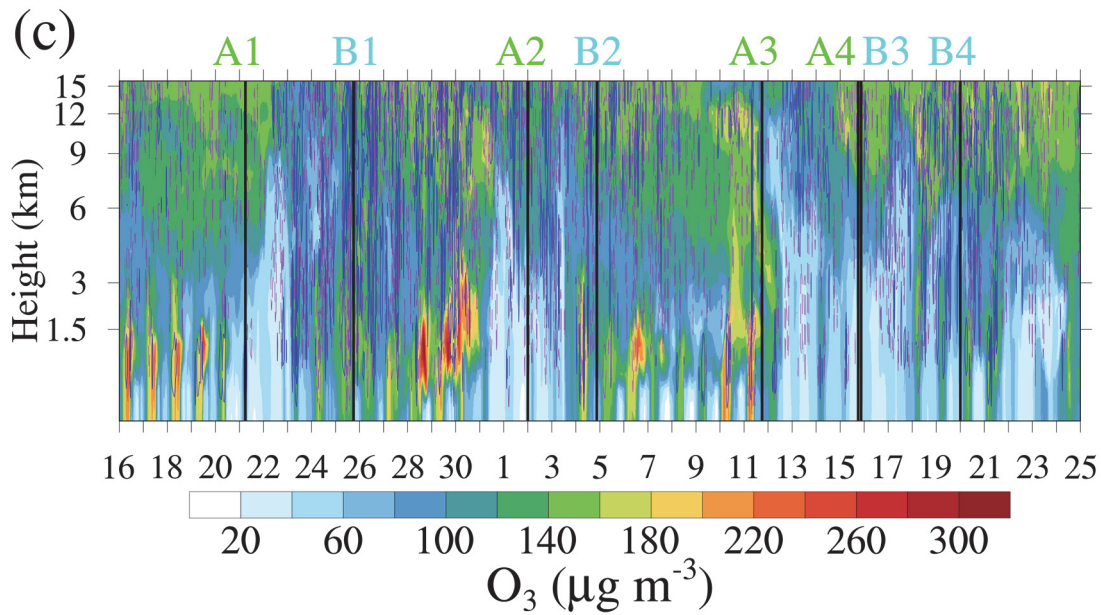


432

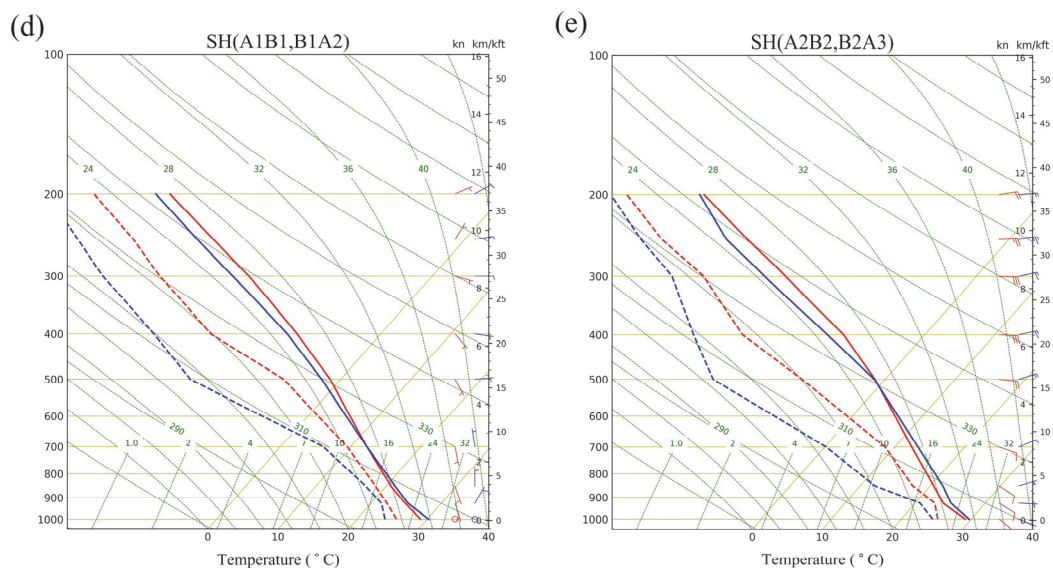


433





434

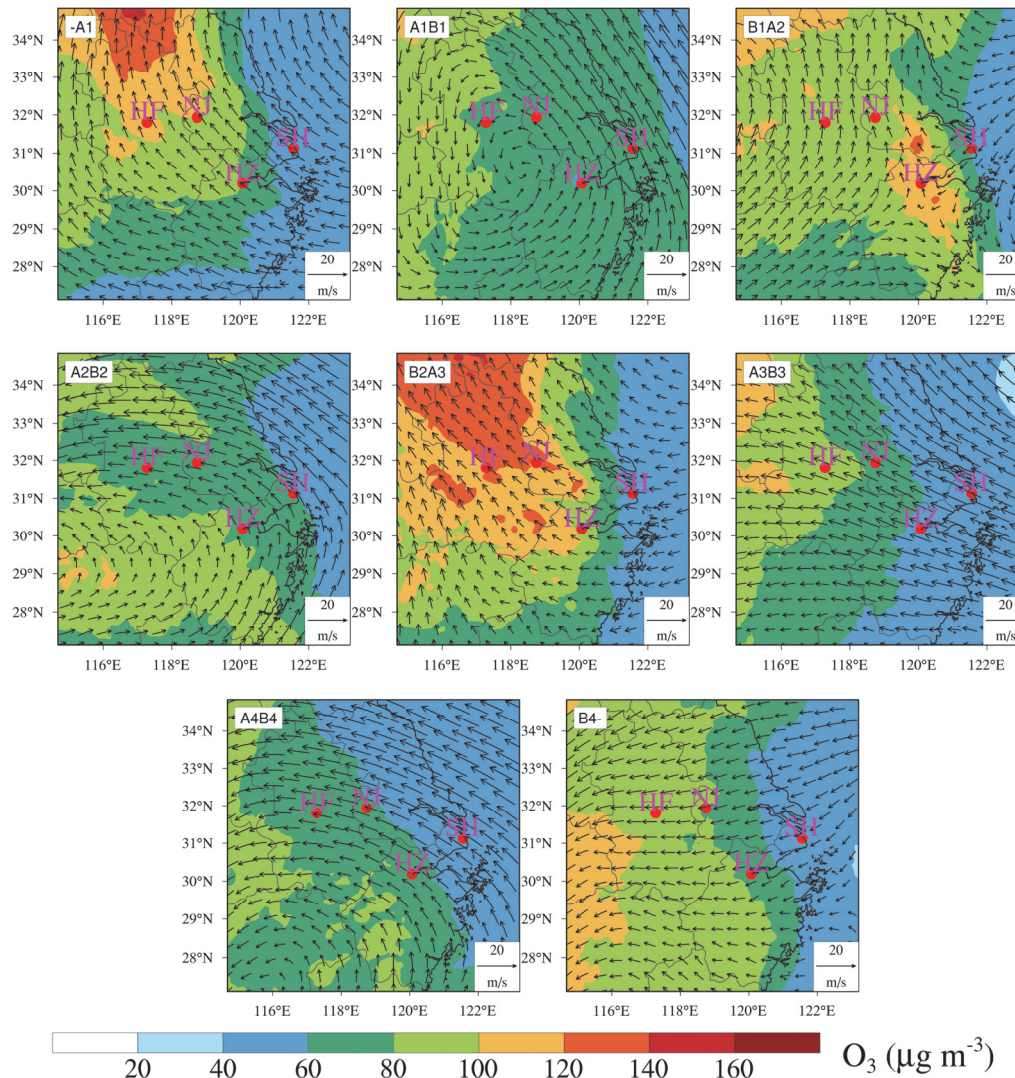


435

436 **Figure 6. (a) Time series of air pollutants (O_3 , $PM_{2.5}$, SO_2 , CO and NO_2) and meteorological**
 437 **factors (T_2 , RH , WS_{10} and WD_{10}) in Shanghai. (b) Individual processes contribution to net O_3**
 438 **density at Shanghai. O_3 is the net increase, MADV is the sum of horizontal advection (HADV)**
 439 **and vertical advection (ZADV), TDIF is the sum of horizontal diffusion (HDIF) and vertical**
 440 **diffusion (VDIF), CHEM is the chemical reaction process, and DDEP is the dry deposition**
 441 **process. The color histograms indicate the results for the layer near the surface, while the solid**
 442 **red lines indicate the average results for all layers below 1500 m. (c) Temporal-vertical**
 443 **distribution of O_3 with vertical wind velocity over Shanghai. The dotted purple line and solid**
 444 **blue line indicate the negative wind speeds (downward airflows) and positive wind speeds**

445 (upward airflows), respectively. (d) The skew-T log-P diagram at Shanghai. The average
446 results of period A1B1 and B1A2 are shown in red and blue, respectively. (e) Same as (d), but
447 for the average results of period A2B2 and B2A3.

448



449

450 **Figure 7. Spatial distribution of surface O₃ overlaid with wind fields at 850 hPa over the YRD.**
451 -A1, A1B1, B1A2, A2B2, B2A3, A3B3, A4B4, B4- are the average results from the beginning
452 to A1, A1 to B1, B1 to A2, A2 to B2, B2 to A3, A3 to B3, A4 to B4, and B4 to the end, respectively.
453 Details can be found in Figure 4.

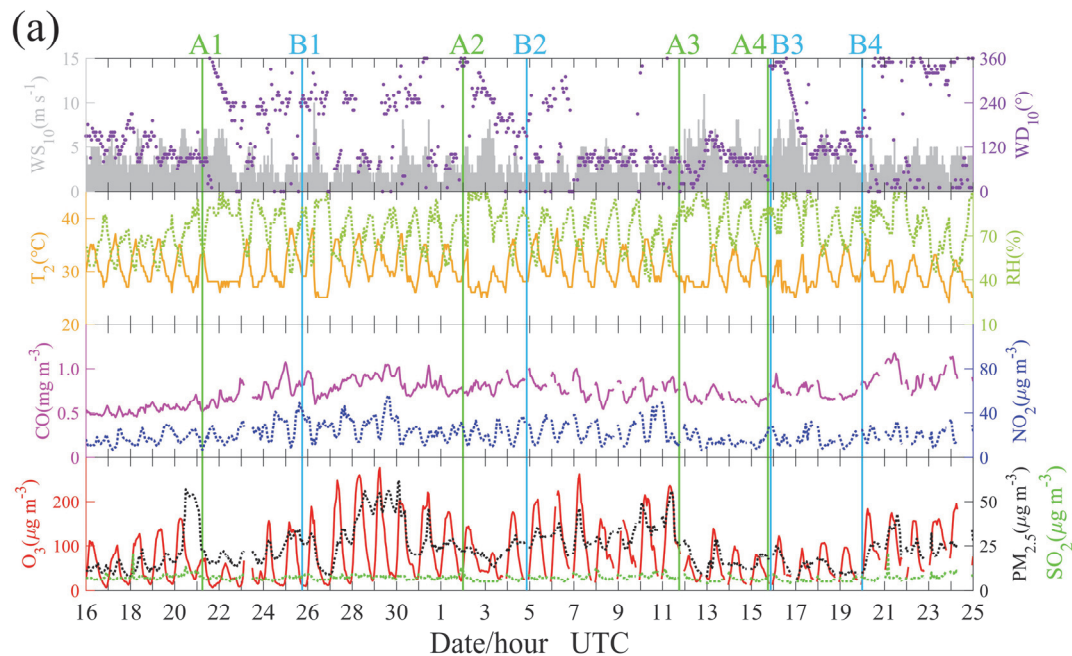
454

455 3.3.3 Hangzhou in category II cities

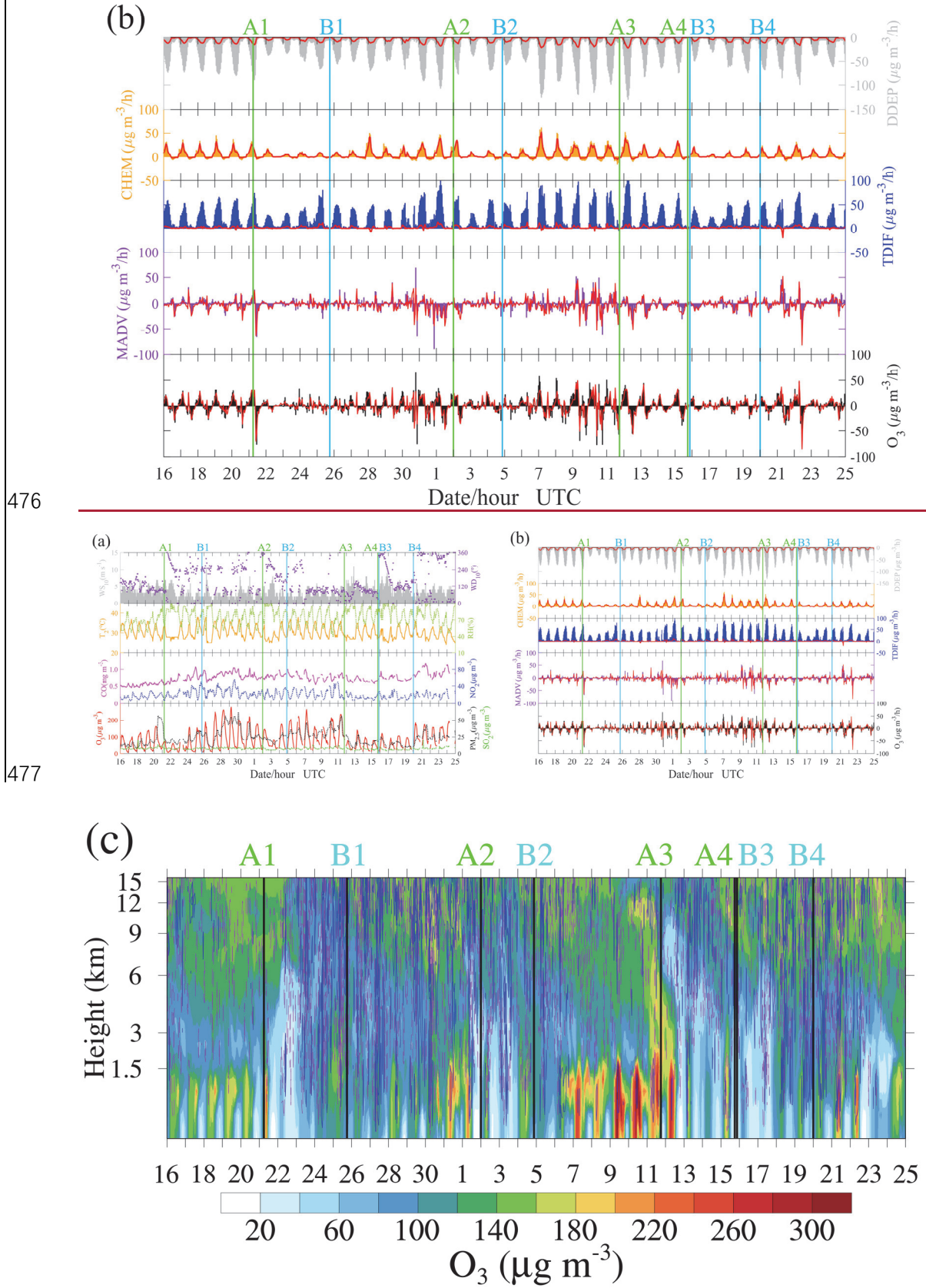
456 Figure 8 presents the case in results for Hangzhou. It shows that high O₃ concentrations
457 occurred on 27-31 July and 5-7 August, which may also be related to the strong photochemical

458 production of O₃ under the abundance of precursors (Figure 8a) and poor diffusion conditions due
 459 to the light wind (B1A2 and B2A3 in Figure 7). Figure 8a further shows that high O₃ was often
 460 associated with an increase in CO but the NO₂ concentrations usually remained at the same level.
 461 This phenomenon indicates a VOCs-limited regime in this city since CO usually have good
 462 correlation with VOCs and can play a similar role as VOCs in the photochemical production of O₃
 463 (Atkinson, 2000; Ding et al., 2013). In fact, O₃ in other representative cities (Shanghai, Nanjing and
 464 Hefei) also showed a better correlation with CO than NO₂. Though Hangzhou is close to Shanghai,
 465 there is a significant difference of wind fields over these two cities. Starting from the arrival of
 466 Typhoon Ampil (A1). The wind direction in Hangzhou did not change back to southeast until a few
 467 days later after Typhoon Jongdari dissipated (B2). During this period (A1B2), the frequent
 468 southwest wind may be the reason for high CO concentrations in Hangzhou. In addition, the chaotic
 469 wind field during period B1A2 (B1A2 in Figure 7) may lead to the light wind in Hangzhou. With
 470 respect to the simulation results, the model simulated the variation of O₃ but failed to capture the O₃
 471 peaks (e.g., the peak values on 27-31 July), which may be related to the strong upward airflows
 472 (Figure 8c) that inhibited the accumulation of O₃ (Figure 8b). This further illustrates that downward
 473 airflows may be an important factor for O₃ episodes in this case.

474



475



478

479 **Figure 8.** Same as Figure 6 (a)-(c), but for Hangzhou.

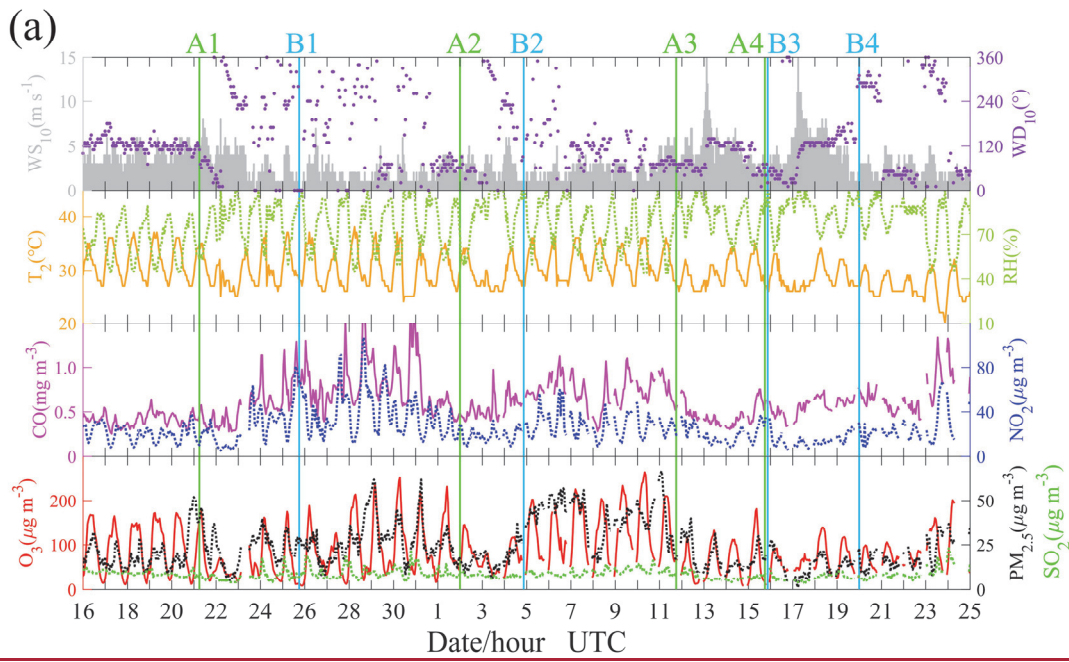
480

481 3.3.4 Nanjing in category III cities

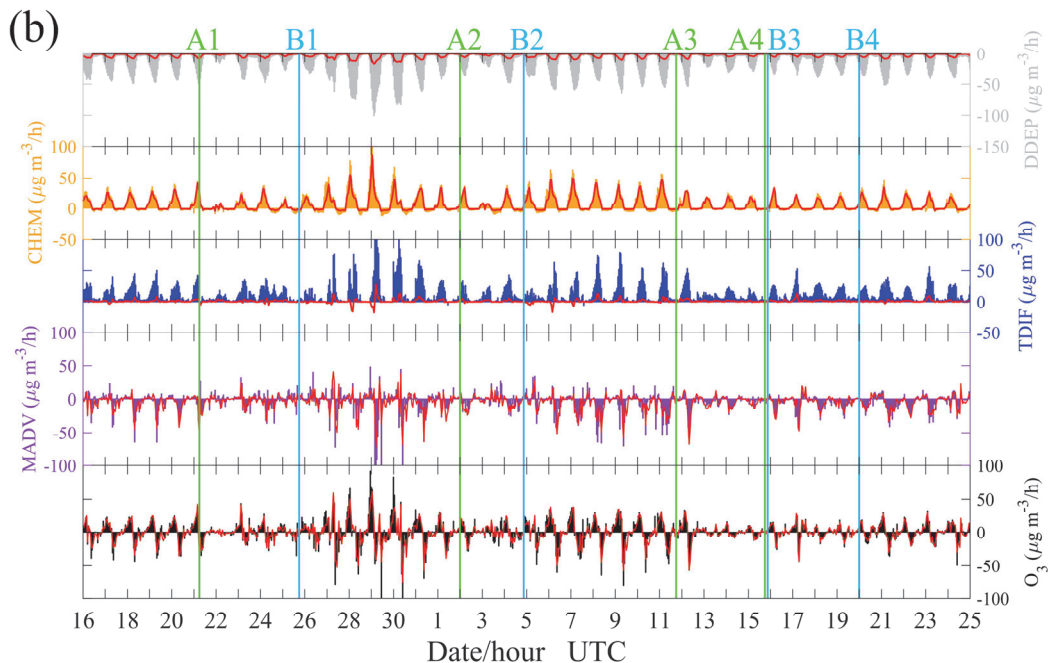
482 ~~In As for~~ Nanjing, the O₃ episodes ~~with~~ exceeded ~~the~~ ~~anee~~ ~~of~~ national air quality standards
483 ~~was~~ ~~ere~~ observed on 28 July to 1 August and 7-11 August. These O₃ episodes were characterized by
484 abundant O₃ precursors under the condition of high temperature. Furthermore, light wind (B1A2
485 and B2A3 in Figure 7) and downward airflows (Figure 9c) also contributed greatly to the occurrence
486 of O₃ pollution, ~~resulting from a mechanism similar to~~ ~~with the similar mechanism as~~ that ~~for~~ ~~of~~
487 Shanghai and Hangzhou. As early as ~~on~~ 22 July, the wind direction in Nanjing ~~had~~ changed from
488 southeast to southwest ~~because of the arrival of~~ ~~affected by~~ Typhoon Ampil, and ~~thus~~ the
489 concentrations of the main primary pollutants (CO, NO₂ and SO₂) increased (Figure 9a). However,
490 high-level O₃ episodes did not occur until 28 July even though the maximum temperature did not
491 change significantly during 24-31 July. The “obstacle” ~~for enhancing O₃ level of the O₃ episodes~~ s
492 may be the precipitation caus~~ed~~ ~~ing~~ by the strong upward airflows during 23-26 July (Figure 9c). As
493 shown in Figure 9b, high surface O₃ concentration during the pollution episodes is the result of
494 TDIF and CHEM processes, and is lost through DDEP and MADV processes. ~~Regarding With~~
495 ~~respect to the~~ vertical structure of atmospheric, B1A2 (B2A3) was also hotter and drier than A1B1
496 (A2B2) below 700 hPa in Nanjing (Figure 9d and 9e). ~~These consequences, similar to those in The~~
497 ~~similar results as~~ Shanghai, further confirm that high O₃ concentrations ~~in a region~~ are more likely
498 to occur during the period from the end of ~~an exciting the~~ typhoon to the arrival of the next typhoon
499 (B1A2 and B2A3) than ~~during~~ the period when ~~at the~~ typhoon approaches and is active in the
500 ~~region mainland China~~ (A1B1 and A2B2).

501

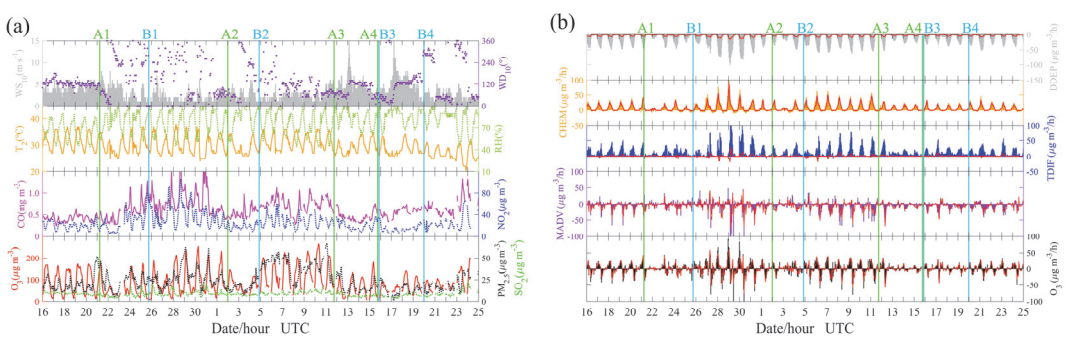
502

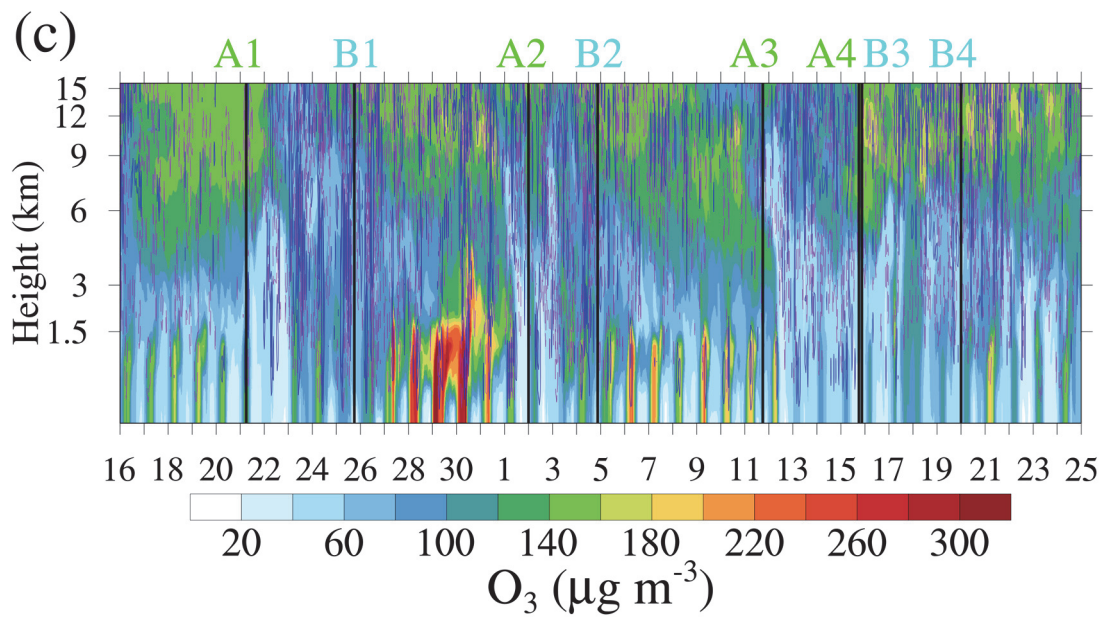


503

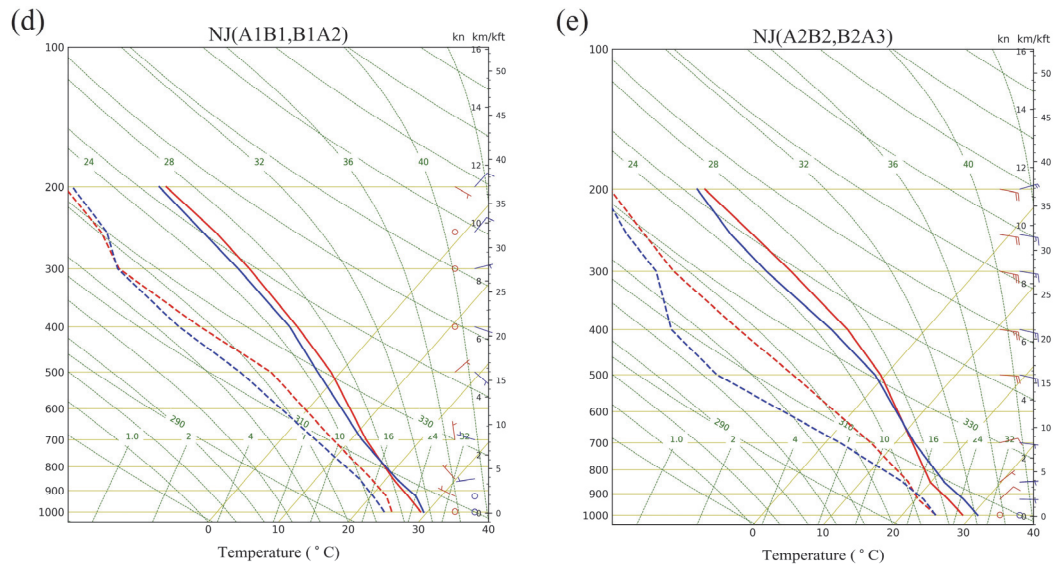


504





505



506

507 **Figure 9. Same as Figure 6, but for Nanjing.**

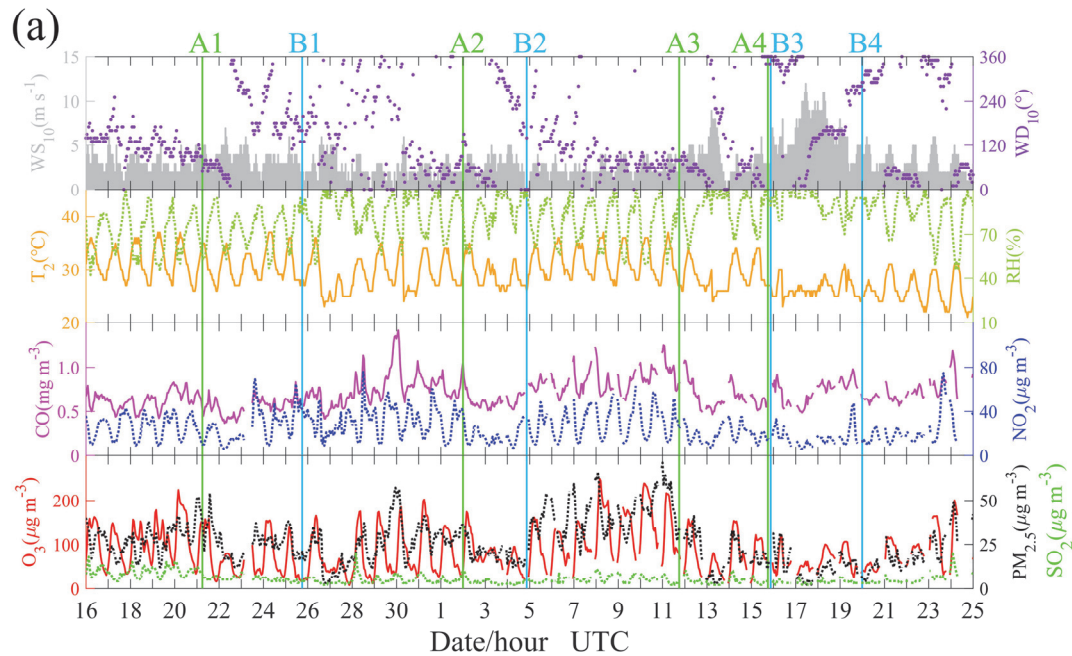
508

509 3.3.5 Hefei in category IV cities

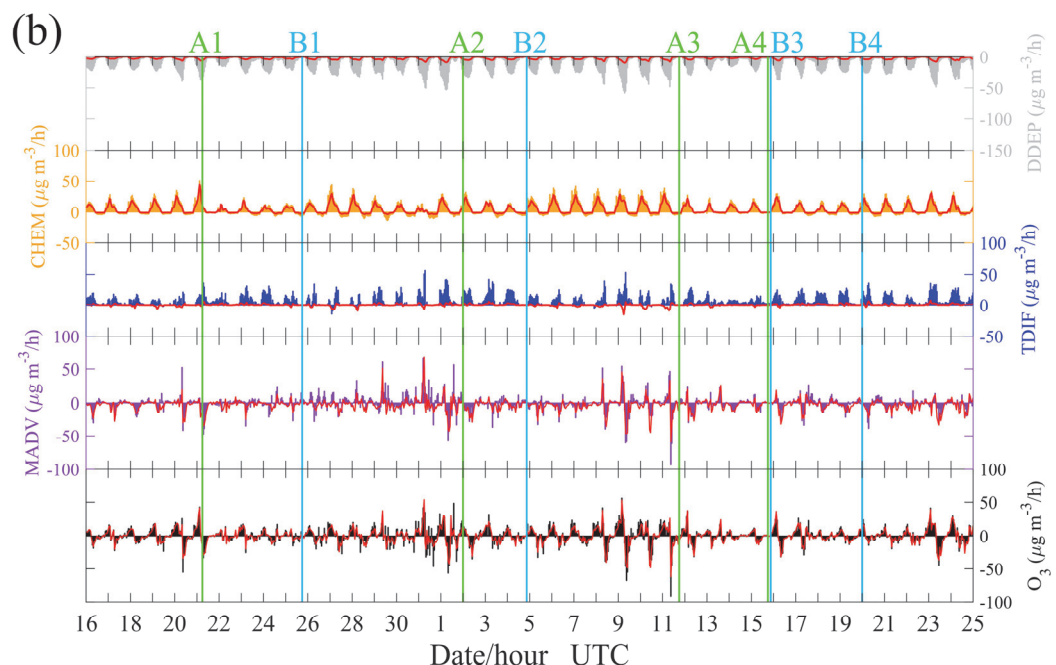
510 Hefei is the city farthest from the coast among the four representative cities, and O_3 pollution
 511 occurred on 31 July and 8-11 August. We ~~can~~ also find the phenomenon that the precursors
 512 concentrations had an increase once the wind direction changed from southeast to southwest (Figure
 513 10a). During B1A2 and B2A3, the concentrations of the main precursors of O_3 washad a high level.
 514 However, high O_3 concentration was mainly found in B2A3, and not in B1A2. This may be related
 515 to the relatively low temperature during B1A2 (Figure 10a), which is not conducive to

516 photochemical production of O₃ (Figure 10b). As shown in Figure 10c, there were distinct upward
 517 airflows within the boundary layer, which may be related to urban effect (e.g., urban heat islands).
 518 These upward airflows within the boundary layer help mix the air, resulting in a uniform distribution
 519 of O₃ in the vertical direction. However, the downward airflows can still inhibit the vertical diffusion
 520 of O₃, and O₃ tends to be trapped within the boundary layer.

521

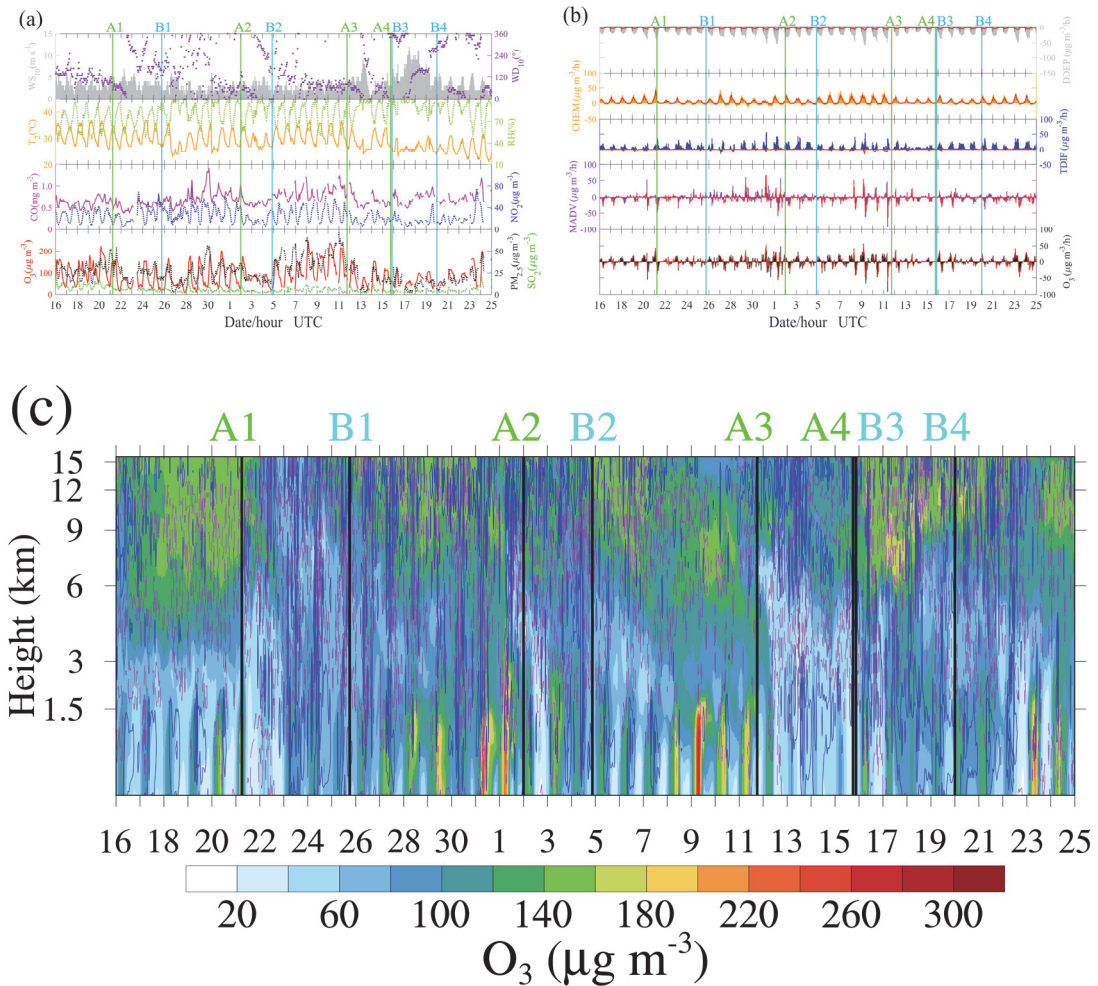


522



523

524



525

526 **Figure 10. Same as Figure 6 (a)-(c), but for Hefei.**

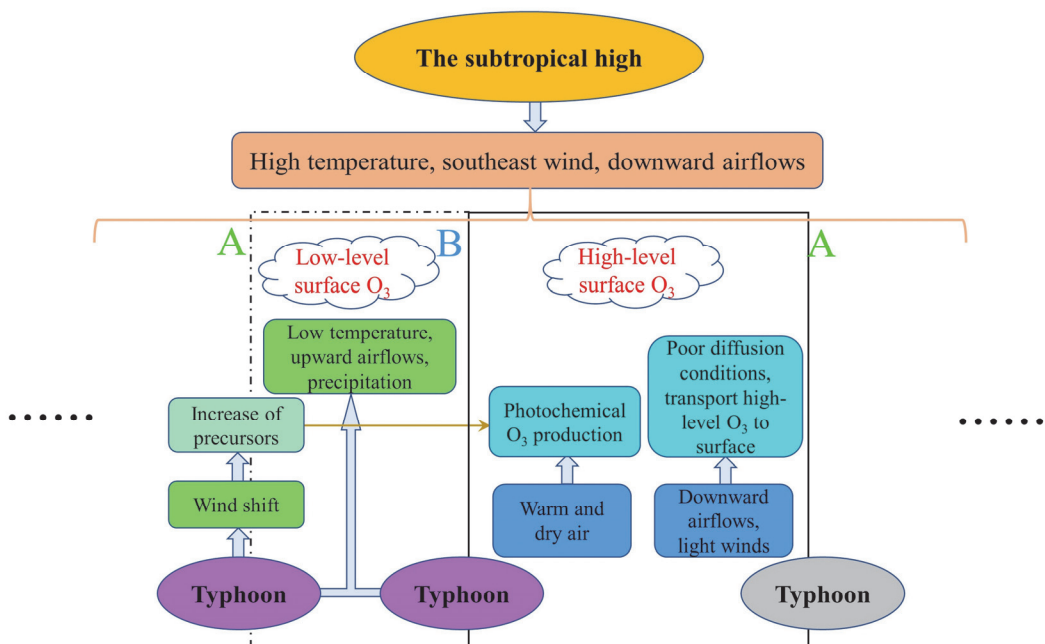
527

528 **3.3.6 A schematic diagram of major processes**

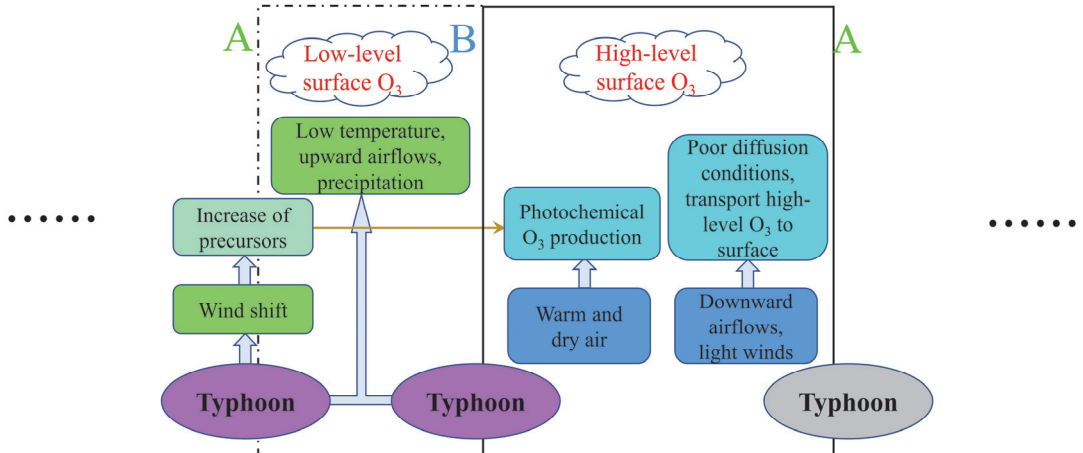
529 Although the processes of landfall typhoon affecting O₃ varied from city to city, the major
 530 processes have many similarities and can be summarized as a schematic diagram in Figure 11. The
 531 YRD region, as a typical region of East Asian monsoon climate, is strongly influenced by typhoon
 532 activities over the Western Pacific The YRD region, which features a typical subtropical monsoon
 533 climate, is strongly influenced by the western Pacific subtropical high in summer. Dominated by the
 534 subtropical high In summer, the meteorological conditions of high temperature and downward
 535 airflows combined with high levels of precursors due to the huge energy consumption tend to form
 536 high O₃-concentrations in this region are all favorable to O₃ accumulation in the region. However,
 537 powerful systems like typhoon can break this state. For typhoons that may land in the YRD, by the
 538 time they approach the 24-hour warning line, the prevailing southeast wind in the YRD will change

539 to southwest wind, which can transport lots of precursors from inland to the YRD. The change in
 540 wind direction depends on the track of the typhoon and the geographical location of cities, and often
 541 appears first in cities along the coastline~~coastal region~~. With influence of a typhoon, the low
 542 temperature, precipitation (upward airflows) and wild windwill prevent high O₃ and PM_{2.5} episodes
 543 from forming. Moreover, the effect of removing pollutants is related to the intensity of typhoon
 544 landing, but some of the main precursors of O₃ are still at a high level due to foreign sources
 545 superposed with local emissions. After the passing of typhoons, the atmosphere returns to a warm
 546 and dry state (even more so than before), and the downward airflows resumed. The troposphere is
 547 then flooded with high O₃ due to two main sources. One is that O₃-rich air transported from the low
 548 stratosphere by the downward airflows, and the other is that O₃ produced by strong photochemical
 549 reactions begin to produce O₃-under the abundance of precursors. O₃ is mainly generated inside the
 550 boundary layer (~1000 m) instead of at the surface. ;The high-level O₃ can remain in the residual
 551 layer at night, and be then transported to the surface by downward airflows or turbulent mixing by
 552 the second day. At the same time, the wind readjusts to southeast and wind speed is light, resulting
 553 in poor diffusion conditions. The downward airflows and light wind obstruct the vertical and
 554 horizontal diffusion of O₃, leaving O₃ trapped on the ground. The thermal-dynamic effects result in
 555 high-level surface O₃ in the YRD.

556



557



558
559 **Figure 11. A schematic diagram of major processes that summertime O₃ is affected by landfall**
560 **typhoons in the YRD. The letter A indicates the moment that the typhoon has reached the 24-**
561 **h warning line, and letter B indicates the last moment when the typhoon remains active.**

562 **in the mainland China.**

563
564 Typhoon can exert an enormous impact on energy transports and air mass in the troposphere
565 as well as redistribution of pollutants. Though In fact, most typhoons generated over the western
566 North Pacific will not land in China, or they are more likely to land in the South China rather than
567 the YRD. In our previous study (Shu et al., 2016), the typhoon did not land in the YRD, but the
568 processes related to high-level O₃ formation may be the same common. That is, the processes
569 shown in the open box enclosed by dashed lines dashed box in Figure 11, which are unique to landfall
570 typhoons, while the processes inside the box enclosed by solid lines in the solid box can be found
571 between typhoons as long as the typhoons that can affect the YRD. Transport of precursors,
572 downward airflows, high temperature and light wind are crucial factors, and how big the roles of
573 those factors play in O₃ episodes depends on behaviors of the typhoons and geographical locations
574 of the city typhoon and city. It is hard to quantify these processes with just a few cases is a large
575 challenge. For example, it is hard to find out we cannot estimate whether the downward airflows are
576 modulated dominated by the subtropical high or the periphery circulation of typhoons since they
577 usually occur simultaneously. Furthermore, the behavior of particulate matter is intriguing since high-
578 level PM_{2.5} often occurs with high-level O₃ after typhoon, which is opposite to the suggestion
579 different from previous studies that high particulate matter concentrations inhibit the formation of

580 O₃ in previous studies (Li et al., 2005; Xing et al., 2017). This may be related to the heterogeneous
581 reactions (Lou et al., 2014) but research on this issue is quite limited to date.

582

583 **3.3 Premature mortalities induced by O₃ exposure**

584 When it comes to typhoons, especially landfall typhoons, the first concern is the huge damage
585 caused by extreme weathers. After the passing of typhoons, people are relieved and go back busy
586 with their lifework as usual. However, our research indicates that high O₃ episodes are likely to
587 occur in the short period after a typhoon landing in the YRD, and high O₃ concentrations can do
588 harm to people's health. To arouse attention on this issue, we estimate the premature mortality
589 attributed to O₃ for respiratory disease, we choose two complete cycles, which is the period A1A3
590 (21 July to 11 August), to do the calculation. In this study, we employ the standard damage function
591 defined by epidemiology studies (Anenverg et al., 2010; Voorhees et al., 2014) to calculate the
592 premature mortalities due to O₃ exposure, the specific formulas and parameters are described in
593 Section 2.7. Table 4 summarized the premature mortalities in cities in the YRD. The premature
594 mortalities are a function of both the population and O₃ levels, resulting in high premature
595 mortalities in populated and heavily polluted areas. Out of the 26 cities in the YRD, Shanghai
596 showed highest premature mortalities (29.2) due to its high surface O₃ concentrations and huge
597 population. The city with the lowest premature mortalities (0.6) was Zhoushan, which may be
598 related to removing effect of the maritime air masses as Zhoushan is located by the sea (Figure 1b).
599 During this period, the total premature mortalities in the YRD was 194.0, which was larger than
600 the number of casualties caused directly by the typhoons (80 people were killed by landfall typhoons
601 in mainland China in 2018).

602

603 **Table 4. Premature mortalities induced by O₃ exposure for respiratory disease**

	City	Population (thousand)	Premature mortalities
Category I cities			
	Shanghai	24,240	29.2
	Yancheng	7,200	6.1
	Nantong	7,310	7.9
	Jiaxing	4,726	7.3
	Ningbo	8,202	8.1
	Zhoushan	1,173	0.6

	Taizhou	6,139	4.1
Category II cities	Hangzhou	9,806	16.5
	Taizhoushi	4,636	5.2
	Changzhou	4,729	4.4
	Wuxi	6,575	10.7
	Suzhou	10,722	15.3
	Huzhou	3,027	2.8
	Shaoxing	5,035	4.7
	Jinhua	5,604	8.2
Category III cities	Nanjing	8,436	13.4
	Yangzhou	4,531	5.5
	Zhenjiang	3,196	5.3
	Chuzhou	4,114	5.8
	Maanshan	2,337	3.6
	Wuhu	3,748	6.2
	Xuancheng	2,648	2.0
Category IV cities	Hefei	8,087	10.9
	Tongling	1,629	1.7
	Chizhou	1,475	2.1
	Anqing	4,691	6.4
	Total	154,016	194.0

604

605

4 Conclusions

606 In this study, we investigate the detail processes of landfall typhoons affecting O₃ in the YRD
 607 based on a unique case ~~from during~~ 16 July to 25 August, 2018, ~~using both with the help of~~
 608 monitoring observations and numerical simulations. This case was characterized by two multiday
 609 regional O₃ pollution episodes ~~involving concerned with~~ four successive landfall typhoons. The two
 610 O₃ episodes appeared from 24 July to 2 August and 5 to 11 August, respectively, with the highest
 611 MDA8 O₃ reached up 264 μg m⁻³.

612 The ~~time when a moment that~~ typhoon reaches the 24-h warning line and the ~~time when the~~
 613 ~~last moment of~~ typhoon ~~dies away activity~~ in the mainland China ~~area~~ crucial, because O₃ pollution
 614 episodes mainly occurred during the period from the end of ~~a~~ typhoon ~~to and~~ the arrival of the next
 615 typhoon in the YRD. These two moments can be roughly regarded as time nodes. Furthermore, it is
 616 found that the variations of O₃ was related to the track, duration and landing intensity of the typhoons
 617 during the study period. O₃ pollution ~~first~~ appeared in ~~cities along the coastline coastal region was~~

618 ahead of that in inland regions due to along the track of the typhoons. The interval between two
619 typhoons can affect the duration of high O₃ concentration in the YRD. Generally, sustained high O₃
620 concentration—likely appeared in the region on days when the existing typhoon had dissipated
621 before the arrival of the next one tends to appear on days when the typhoon has dissipated but not
622 influenced by the new one. Regarding the impact of As for the landing intensity of typhoon, the
623 stronger the typhoon landed, the gale and precipitation accompanying the typhoon would be more
624 effective in suppressing O₃ generation removing O₃, resulting in lower O₃ concentration in the
625 typhoon landing location.

626 The detail processes of landfall typhoons affecting O₃ depend on typhoons and cities. High
627 temperature and downward airflows dominated by the subtropical high combined with abundant
628 precursors are the main reasons for high O₃ concentration in the YRD in summer. And landfall
629 typhoons can change this state through the following mechanism: When the landfall typhoon is
630 close enough (~24-hour warning line), the prevailing southeast wind will change to southwest wind,
631 which transports large amount of precursors from inland to the YRD. The southwest wind usually
632 appears first in coastal regions, and the wind direction will turn back to southeast wind as long as
633 the YRD is dominated by the subtropical high. Then the typhoon makes landfall, the low
634 temperature, precipitation (upward airflows) and wild wind suppress the generation of O₃. After the
635 typhoon passing, the atmosphere in at low layers (below 700 hPa) will be warm and dry, and
636 downward airflows resume. The troposphere is likely to fill with high concentration of O₃ due to
637 O₃-rich air transported from the low stratosphere and strong photochemical reactions begin to
638 produce O₃ under the abundance of precursors due to foreign sources superposed with local
639 emissions. O₃ is mainly generated in the middle of boundary layer (~1000 m) instead of at the
640 surface. The high-level O₃ can remain in the residual layer at night, and can be then transported to
641 the surface by downward airflows or turbulent mixing by the second day. The downward airflows
642 also obstruct the vertical diffusion of O₃. Meanwhile, wind speed is light when the wind readjusts
643 to southeast, which further reduces worsens horizontal diffusion of O₃. Thus, The O₃ can be
644 accumulated and trapped on the ground. The thermal-dynamic effects results in high surface O₃
645 concentration in the YRD. Those processes will repeat if the next typhoon approaches.

646 The estimated premature mortalities attributed to O₃ exposure for respiratory disease in the
647 YRD during 21 July to 11 August (two complete cycles of typhoons) was 194.0, which is larger

648 than the number of casualties caused directly by the typhoons. This work ~~has~~enhanced our
649 understanding of how landfall typhoons affect O₃ in the YRD, which may help ~~synthetically to~~
650 forecast ~~the~~ O₃ pollution ~~modulated synthetically impacted~~ by the subtropical high and typhoons.
651 Meanwhile, our results further confirm that large-scale synoptic weather systems play an important
652 role in regional air pollution, suggesting a need in establishing potential links between air pollution
653 and predominant synoptic weather patterns.

654

655 **Author contributions.** C. C. Zhan and M. Xie had the original ideas, designed the research, collected
656 the data, and prepared the original draft. C. C. Zhan carried out the data analysis. M. Xie acquired
657 financial support for the project leading to this publication. C. W. Huang taught and helped C. C.
658 Zhan to do the numerical simulation. J. Liu and T. J. Wang ~~and J. Liu~~ revised the manuscript and
659 helped to collect the data. C. Q. Ma helped to deal with the emission inventory. M. Xu and J. W. Yu
660 helped to collect the data. M. M. Li, S. Li, B. L. Zhuang, and M. Zhao reviewed the initial draft and
661 checked the English of the original manuscript. Y. M. Jiao and D. Y. Nie reviewed the initial draft
662 and helped to improve the work of health impact.

663

664 **Acknowledgements.**

665 This work was supported by the National Key Research and Development Program of China
666 (2018YFC0213502, 2018YFC1506404), the open research fund of Chongqing Meteorological
667 Bureau (KFJJ-201607) and the Fundamental Research Funds for the Central Universities
668 (020714380047).

669

670 **References**

- 671 Allen, R. J., Sherwood, S. C., Norris, J. R., and Zender, C. S.: Recent Northern Hemisphere tropical
672 expansion primarily driven by black carbon and tropospheric ozone, *Nature*, 485, 350-354,
673 10.1038/nature11097, 2012.
- 674 Anenberg, S. C., Horowitz, L. W., Tong, D. Q., and West, J. J.: An estimate of the global burden of
675 anthropogenic ozone and fine particulate matter on premature human mortality using
676 atmospheric modeling, *Environ Health Perspect*, 118, 1189-1195, 10.1289/ehp.0901220, 2010.
- 677 Burnett, R. T., Pope, C. A., 3rd, Ezzati, M., Olives, C., Lim, S. S., Mehta, S., Shin, H. H., Singh, G.,

- 678 Hubbell, B., Brauer, M., Anderson, H. R., Smith, K. R., Balmes, J. R., Bruce, N. G., Kan, H.,
679 Laden, F., Pruss-Ustun, A., Turner, M. C., Gapstur, S. M., Diver, W. R., and Cohen, A.: An
680 integrated risk function for estimating the global burden of disease attributable to ambient fine
681 particulate matter exposure, *Environ Health Perspect*, 122, 397-403, 10.1289/ehp.1307049,
682 2014.
- 683 Chameides, W., and Walker, J. C. G.: A photochemical theory of tropospheric ozone, *Journal of*
684 *Geophysical Research*, 78, 8751-8760, 10.1029/JC078i036p08751, 1973.
- 685 Chan, C. K., and Yao, X.: Air pollution in mega cities in China, *Atmospheric Environment*, 42, 1-
686 42, 10.1016/j.atmosenv.2007.09.003, 2008.
- 687 Deng, T., Wang, T., Wang, S., Zou, Y., Yin, C., Li, F., Liu, L., Wang, N., Song, L., Wu, C., and Wu,
688 D.: Impact of typhoon periphery on high ozone and high aerosol pollution in the Pearl River
689 Delta region, *The Science of the total environment*, 668, 617-630,
690 10.1016/j.scitotenv.2019.02.450, 2019.
- 691 Ding, A. J., Wang, T., Thouret, V., Cammas, J. P., and Nedelec, P.: Tropospheric ozone climatology
692 over Beijing: analysis of aircraft data from the MOZAIC program, *Atmospheric Chemistry and*
693 *Physics*, 8, 1-13, 2008.
- 694 Ding, A. J., Fu, C. B., Yang, X. Q., Sun, J. N., Zheng, L. F., Xie, Y. N., Herrmann, E., Nie, W., Petäjä,
695 T., Kerminen, V. M., and Kulmala, M.: Ozone and fine particle in the western Yangtze River
696 Delta: an overview of 1 yr data at the SORPES station, *Atmospheric Chemistry and Physics*,
697 13, 5813-5830, 10.5194/acp-13-5813-2013, 2013.
- 698 Ding, A., Nie, W., Huang, X., Chi, X., Sun, J., Kerminen, V.-M., Xu, Z., Guo, W., Petäjä, T., Yang,
699 X., Kulmala, M., and Fu, C.: Long-term observation of air pollution-weather/climate
700 interactions at the SORPES station: a review and outlook, *Frontiers of Environmental Science*
701 & Engineering, 10, 10.1007/s11783-016-0877-3, 2016.
- 702 Dong J Y, Liu X R, Zhang B Z.: Meta-analysis of association between short-term ozone exposure
703 and population mortality in China, *Acta Scientiae Circumstantiae*, 36 (4), 1477-1485, 2016 (in
704 Chinese).
- 705 Fan, Q., Lan, J., Liu, Y. M., Wang, X. M., Chan, P. W., Hong, Y. Y., Feng, Y. R., Liu, Y. X., Zeng, Y.
706 J., and Liang, G. X.: Process analysis of regional aerosol pollution during spring in the Pearl
707 River Delta region, China, *Atmospheric Environment*, 122, 829-838, 2015.

- 708 Ghude, S. D., Chate, D. M., Jena, C., Beig, G., Kumar, R., Barth, M. C., Pfister, G. G., Fadnavis, S.,
709 and Pithani, P.: Premature mortality in India due to PM_{2.5} and ozone exposure, Geophys Res
710 Lett, 43, 4650-4658, 10.1002/2016gl068949, 2016.
- 711 Guo, S., Hu, M., Zamora, M. L., Peng, J., Shang, D., Zheng, J., Du, Z., Wu, Z., Shao, M., Zeng, L.,
712 Molina, M. J., and Zhang, R.: Elucidating severe urban haze formation in China, Proceedings
713 of the National Academy of Sciences of the United States of America, 111, 17373-17378,
714 10.1073/pnas.1419604111, 2014.
- 715 Hu, J., Chen, J., Ying, Q., and Zhang, H.: One-year simulation of ozone and particulate matter in
716 China using WRF/CMAQ modeling system, Atmospheric Chemistry and Physics, 16, 10333-
717 10350, 10.5194/acp-16-10333-2016, 2016.
- 718 Huang, J.-P.: Numerical simulation and process analysis of typhoon-related ozone episodes in Hong
719 Kong, Journal of Geophysical Research, 110, 10.1029/2004jd004914, 2005.
- 720 Huang, R. J., Zhang, Y., Bozzetti, C., Ho, K. F., Cao, J. J., Han, Y., Daellenbach, K. R., Slowik, J.
721 G., Platt, S. M., Canonaco, F., Zotter, P., Wolf, R., Pieber, S. M., Bruns, E. A., Crippa, M.,
722 Ciarelli, G., Piazzalunga, A., Schwikowski, M., Abbaszade, G., Schnelle-Kreis, J.,
723 Zimmermann, R., An, Z., Szidat, S., Baltensperger, U., El Haddad, I., and Prevot, A. S.: High
724 secondary aerosol contribution to particulate pollution during haze events in China, Nature,
725 514, 218-222, 10.1038/nature13774, 2014.
- 726 Jerrett, M., Burnett, R. T., Pope, C. A., Ito, K., Thurston, G., Krewski, D., Shi, Y. L., Calle, E., and
727 Thun, M.: Long-Term Ozone Exposure and Mortality., New Engl J Med, 360, 1085-1095, 2009.
- 728 Jiang, Y. C., Zhao, T. L., Liu, J., Xu, X. D., Tan, C. H., Cheng, X. H., Bi, X. Y., Gan, J. B., You, J.
729 F., and Zhao, S. Z.: Why does surface ozone peak before a typhoon landing in southeast China?,
730 Atmospheric Chemistry and Physics, 15, 13331-13338, 10.5194/acp-15-13331-2015, 2015.
- 731 Jiménez, P. A., and Dudhia, J.: Improving the Representation of Resolved and Unresolved
732 Topographic Effects on Surface Wind in the WRF Model, Journal of Applied Meteorology and
733 Climatology, 51, 300-316, 10.1175/jamc-d-11-084.1, 2012.
- 734 Jin, Y., Andersson, H., and Zhang, S.: Air Pollution Control Policies in China: A Retrospective and
735 Prospects, Int J Environ Res Public Health, 13, 10.3390/ijerph13121219, 2016.
- 736 Kamens, R., Jang, M., Chien, C. J., and Leach, K.: Aerosol formation from the reaction of alpha-
737 pinene and ozone using a gas-phase kinetics aerosol partitioning model, Environmental

- 738 Science & Technology, 33, 1430-1438, 1999.
- 739 Kan, H., Chen, R., and Tong, S.: Ambient air pollution, climate change, and population health in
740 China, Environ Int, 42, 10-19, 10.1016/j.envint.2011.03.003, 2012.
- 741 Khoder, M. I.: Atmospheric conversion of sulfur dioxide to particulate sulfate and nitrogen dioxide
742 to particulate nitrate and gaseous nitric acid in an urban area, Chemosphere, 49, 675-684, 2002.
- 743 Lelieveld, J., Evans, J. S., Fnais, M., Giannadaki, D., and Pozzer, A.: The contribution of outdoor
744 air pollution sources to premature mortality on a global scale, Nature, 525, 367-371,
745 10.1038/nature15371, 2015.
- 746 Li, L., Chen, C. H., Fu, J. S., Huang, C., Streets, D. G., Huang, H. Y., Zhang, G. F., Wang, Y. J.,
747 Jang, C. J., Wang, H. L., Chen, Y. R., and Fu, J. M.: Air quality and emissions in the Yangtze
748 River Delta, China, Atmospheric Chemistry and Physics, 11, 1621-1639, 10.5194/acp-11-
749 1621-2011, 2011.
- 750 Li, L., Chen, C. H., Huang, C., Huang, H. Y., Zhang, G. F., Wang, Y. J., Wang, H. L., Lou, S. R.,
751 Qiao, L. P., Zhou, M., Chen, M. H., Chen, Y. R., Streets, D. G., Fu, J. S., and Jang, C. J.: Process
752 analysis of regional ozone formation over the Yangtze River Delta, China using the Community
753 Multi-scale Air Quality modeling system, Atmospheric Chemistry and Physics, 12, 10971-
754 10987, 2012.
- 755 Li, S. H., and Hong, H. P.: Typhoon wind hazard estimation for China using an empirical track
756 model, Natural Hazards, 82, 1009-1029, 10.1007/s11069-016-2231-2, 2016.
- 757 Li, M., Liu, H., Geng, G., Hong, C., Liu, F., Song, Y., Tong, D., Zheng, B., Cui, H., Man, H., Zhang,
758 Q., and He, K.: Anthropogenic emission inventories in China: a review, National Science
759 Review, 4, 834-866, 10.1093/nsr/nwx150, 2017.
- 760 Li, M., Wang, T., Xie, M., Zhuang, B., Li, S., Han, Y., and Chen, P.: Impacts of aerosol-radiation
761 feedback on local air quality during a severe haze episode in Nanjing megacity, eastern China,
762 Tellus B: Chemical and Physical Meteorology, 69, 10.1080/16000889.2017.1339548, 2017.
- 763 Li, M., Wang, T., Xie, M., Zhuang, B., Li, S., Han, Y., Song, Y., and Cheng, N.: Improved
764 meteorology and ozone air quality simulations using MODIS land surface parameters in the
765 Yangtze River Delta urban cluster, China, Journal of Geophysical Research: Atmospheres, 122,
766 3116-3140, 10.1002/2016jd026182, 2017.
- 767 Li, S., Wang, T., Huang, X., Pu, X., Li, M., Chen, P., Yang, X.-Q., and Wang, M.: Impact of East

- 768 Asian Summer Monsoon on Surface Ozone Pattern in China, Journal of Geophysical Research:
769 Atmospheres, 123, 1401-1411, 10.1002/2017jd027190, 2018.
- 770 Li, M., Wang, T., Xie, M., Li, S., Zhuang, B., Huang, X., Chen, P., Zhao, M., and Liu, J.: Formation
771 and Evolution Mechanisms for Two Extreme Haze Episodes in the Yangtze River Delta Region
772 of China During Winter 2016, Journal of Geophysical Research: Atmospheres, 124, 3607-3623,
773 10.1029/2019jd030535, 2019.
- 774 Liao, J., Wang, T., Jiang, Z., Zhuang, B., Xie, M., Yin, C., Wang, X., Zhu, J., Fu, Y., and Zhang, Y.:
775 WRF/Chem modeling of the impacts of urban expansion on regional climate and air pollutants
776 in Yangtze River Delta, China, Atmospheric Environment, 106, 204-214,
777 10.1016/j.atmosenv.2015.01.059, 2015.
- 778 Liao, Z., Gao, M., Sun, J., and Fan, S.: The impact of synoptic circulation on air quality and
779 pollution-related human health in the Yangtze River Delta region, The Science of the total
780 environment, 607-608, 838-846, 10.1016/j.scitotenv.2017.07.031, 2017.
- 781 Liu, D., Pang, L., and Xie, B.: Typhoon disaster in China: prediction, prevention, and mitigation,
782 Natural Hazards, 49, 421-436, 10.1007/s11069-008-9262-2, 2009.
- 783 Liu, H., Liu, S., Xue, B. R., Lv, Z. F., Meng, Z. H., Yang, X. F., Xue, T., Yu, Q., and He, K. B.:
784 Ground-level ozone pollution and its health impacts in China, Atmospheric Environment, 173,
785 223-230, 2018.
- 786 Lou, S., Liao, H., and Zhu, B.: Impacts of aerosols on surface-layer ozone concentrations in China
787 through heterogeneous reactions and changes in photolysis rates, Atmospheric Environment,
788 85, 123-138, 10.1016/j.atmosenv.2013.12.004, 2014.
- 789 Lu, X., Hong, J., Zhang, L., Cooper, O. R., Schultz, M. G., Xu, X., Wang, T., Gao, M., Zhao, Y., and
790 Zhang, Y.: Severe Surface Ozone Pollution in China: A Global Perspective, Environmental
791 Science & Technology Letters, 5, 487-494, 10.1021/acs.estlett.8b00366, 2018.
- 792 Monks, P. S., Archibald, A. T., Colette, A., Cooper, O., Coyle, M., Derwent, R., Fowler, D., Granier,
793 C., Law, K. S., Mills, G. E., Stevenson, D. S., Tarasova, O., Thouret, V., von Schneidemesser,
794 E., Sommariva, R., Wild, O., and Williams, M. L.: Tropospheric ozone and its precursors from
795 the urban to the global scale from air quality to short-lived climate forcer, Atmospheric
796 Chemistry and Physics, 15, 8889-8973, 10.5194/acp-15-8889-2015, 2015.
- 797 Shu, L., Xie, M., Wang, T., Gao, D., Chen, P., Han, Y., Li, S., Zhuang, B., and Li, M.: Integrated

- 798 studies of a regional ozone pollution synthetically affected by subtropical high and typhoon
799 system in the Yangtze River Delta region, China, Atmospheric Chemistry and Physics, 16,
800 15801-15819, 10.5194/acp-16-15801-2016, 2016.
- 801 Shu, L., Xie, M., Gao, D., Wang, T., Fang, D., Liu, Q., Huang, A., and Peng, L.: Regional severe
802 particle pollution and its association with synoptic weather patterns in the Yangtze River Delta
803 region, China, Atmospheric Chemistry and Physics, 17, 12871-12891, 10.5194/acp-17-12871-
804 2017, 2017.
- 805 Tang, X.Y., Li, J.L., Dong, Z.X., Wang, Y.Y., Wang, W.X., Qi, L.W., Liu, X.L., Zhang, Y.T., Zhang,
806 X.J., Tian, B.S., Jin, S.W., Yang, L.Q., Zhang, Y.X., 1989. Photochemical pollution in Lanzhou,
807 China - a case study. *J. Environ. Sci. China* 1, 31e38.
- 808 Van Dingenen, R., Dentener, F. J., Raes, F., Krol, M. C., Emberson, L., and Cofala, J.: The global
809 impact of ozone on agricultural crop yields under current and future air quality legislation,
810 Atmospheric Environment, 43, 604-618, 10.1016/j.atmosenv.2008.10.033, 2009.
- 811 Voorhees, A. S., Wang, J., Wang, C., Zhao, B., Wang, S., and Kan, H.: Public health benefits of
812 reducing air pollution in Shanghai: a proof-of-concept methodology with application to
813 BenMAP, *The Science of the total environment*, 485-486, 396-405,
814 10.1016/j.scitotenv.2014.03.113, 2014.
- 815 Wang, T., and Kwok, J. Y. H.: Measurement and analysis of a multiday photochemical smog episode
816 in the Pearl River delta of China, *J Appl Meteorol*, 42, 404-416, 2003.
- 817 Wang, X., Zhang, Y., Hu, Y., Zhou, W., Lu, K., Zhong, L., Zeng, L., Shao, M., Hu, M., and Russell,
818 A. G.: Process analysis and sensitivity study of regional ozone formation over the Pearl River
819 Delta, China, during the PRIDE-PRD2004 campaign using the Community Multiscale Air
820 Quality modeling system, Atmospheric Chemistry and Physics, 10, 4423-4437, 10.5194/acp-
821 10-4423-2010, 2010.
- 822 Wang, M., Cao, C., Li, G., and Singh, R. P.: Analysis of a severe prolonged regional haze episode
823 in the Yangtze River Delta, China, *Atmospheric Environment*, 102, 112-121,
824 10.1016/j.atmosenv.2014.11.038, 2015.
- 825 Wang, T., Xue, L., Brimblecombe, P., Lam, Y. F., Li, L., and Zhang, L.: Ozone pollution in China:
826 A review of concentrations, meteorological influences, chemical precursors, and effects, *The
827 Science of the total environment*, 575, 1582-1596, 10.1016/j.scitotenv.2016.10.081, 2017.

- 828 Wang, T., Gao, T., Zhang, H., Ge, M., Lei, H., Zhang, P., Zhang, P., Lu, C., Liu, C., Zhang, H.,
829 Zhang, Q., Liao, H., Kan, H., Feng, Z., Zhang, Y., Qie, X., Cai, X., Li, M., Liu, L., and Tong,
830 S.: Review of Chinese atmospheric science research over the past 70 years: Atmospheric
831 physics and atmospheric environment, *Science China Earth Sciences*, 62, 1903-1945,
832 10.1007/s11430-019-9536-1, 2019.
- 833 Wei, X., Lam, K.-s., Cao, C., Li, H., and He, J.: Dynamics of the Typhoon Haitang Related High
834 Ozone Episode over Hong Kong, *Advances in Meteorology*, 2016, 1-12,
835 10.1155/2016/6089154, 2016.
- 836 Xie, M., Zhu, K., Wang, T., Yang, H., Zhuang, B., Li, S., Li, M., Zhu, X., and Ouyang, Y.:
837 Application of photochemical indicators to evaluate ozone nonlinear chemistry and pollution
838 control countermeasure in China, *Atmospheric Environment*, 99, 466-473,
839 10.1016/j.atmosenv.2014.10.013, 2014.
- 840 Xie, M., Liao, J., Wang, T., Zhu, K., Zhuang, B., Han, Y., Li, M., and Li, S.: Modeling of the
841 anthropogenic heat flux and its effect on regional meteorology and air quality over the Yangtze
842 River Delta region, China, *Atmospheric Chemistry and Physics*, 16, 6071-6089, 10.5194/acp-
843 16-6071-2016, 2016.
- 844 Xie, M., Zhu, K., Wang, T., Chen, P., Han, Y., Li, S., Zhuang, B., and Shu, L.: Temporal
845 characterization and regional contribution to O₃ and NO_x at an urban and a suburban site in
846 Nanjing, China, *The Science of the total environment*, 551-552, 533-545,
847 10.1016/j.scitotenv.2016.02.047, 2016.
- 848 Xie, M., Shu, L., Wang, T.-j., Liu, Q., Gao, D., Li, S., Zhuang, B.-l., Han, Y., Li, M.-m., and Chen,
849 P.-l.: Natural emissions under future climate condition and their effects on surface ozone in the
850 Yangtze River Delta region, China, *Atmospheric Environment*, 150, 162-180,
851 10.1016/j.atmosenv.2016.11.053, 2017.
- 852 Xu, X., Lin, W., Wang, T., Yan, P., Tang, J., Meng, Z., and Wang, Y.: Long-term trend of surface
853 ozone at a regional background station in eastern China 1991-2006: enhanced variability,
854 *Atmospheric Chemistry and Physics*, 8, 2595-2607, 2008.
- 855 Xue, L. K., Wang, T., Gao, J., Ding, A. J., Zhou, X. H., Blake, D. R., Wang, X. F., Saunders, S. M.,
856 Fan, S. J., Zuo, H. C., Zhang, Q. Z., and Wang, W. X.: Ground-level ozone in four Chinese
857 cities: precursors, regional transport and heterogeneous processes, *Atmospheric Chemistry and*

- 858 Physics, 14, 13175-13188, 10.5194/acp-14-13175-2014, 2014.
- 859 Yang, J. X., Lau, A. K. H., Fung, J. C. H., Zhou, W., and Wenig, M.: An air pollution episode and
860 its formation mechanism during the tropical cyclone Nuri's landfall in a coastal city of south
861 China, Atmospheric Environment, 54, 746-753, 10.1016/j.atmosenv.2011.12.023, 2012.
- 862 Ying, M., Zhang, W., Yu, H., Lu, X., Feng, J., Fan, Y., Zhu, Y., and Chen, D.: An Overview of the
863 China Meteorological Administration Tropical Cyclone Database, Journal of Atmospheric and
864 Oceanic Technology, 31, 287-301, 10.1175/jtech-d-12-00119.1, 2014.
- 865 Zhan, C.-c., Xie, M., Fang, D.-x., Wang, T.-j., Wu, Z., Lu, H., Li, M.-m., Chen, P.-l., Zhuang, B.-l.,
866 Li, S., Zhang, Z.-q., Gao, D., Ren, J.-y., and Zhao, M.: Synoptic weather patterns and their
867 impacts on regional particle pollution in the city cluster of the Sichuan Basin, China,
868 Atmospheric Environment, 208, 34-47, 10.1016/j.atmosenv.2019.03.033, 2019.
- 869 Zhang, Q. A., Wu, L. G., and Liu, Q. F.: Tropical Cyclone Damages in China 1983-2006, Bulletin
870 of the American Meteorological Society, 90, 489-+, 2009.
- 871 Zhao, C., Wang, Y., Yang, Q., Fu, R., Cunnold, D., and Choi, Y.: Impact of East Asian summer
872 monsoon on the air quality over China: View from space, Journal of Geophysical Research,
873 115, 10.1029/2009jd012745, 2010.
- 874 Zhao, K., Li, X., Xue, M., Jou, B. J.-D., and Lee, W.-C.: Short-term forecasting through intermittent
875 assimilation of data from Taiwan and mainland China coastal radars for Typhoon Meranti
876 (2010) at landfall, Journal of Geophysical Research: Atmospheres, 117, n/a-n/a,
877 10.1029/2011jd017109, 2012.
- 878